The Stability of Unsaturated Lateritic Slopes Under Rainfall Conditions Considering Shear Strength Variability

A Estabilidade de Taludes Lateríticos Não Saturados em Condições de Chuva Considerando a Variabilidade da Resistência ao Cisalhamento

Pedro Henrique Lopes Dal-Cól[ad], Alana Dias de Oliveira[be], Gilson de Farias Neves Gitirana Junior[cf], Raquel Souza Teixeira[ag]

[a]Universidade Estadual de Londrina, [b]Universidade Tecnológica Federal do Paraná, [c]Universidade Federal de Goiás
[d]eng.pedro.dalcol@uel.br, [e]alanaoliveira@utfpr.edu.br, [f]gilsongitirana@ufg.br, [g]raquel@uel.br

Abstract

Rainfall-induced slope failures pose significant risks and economic impacts globally. This study investigates the impact of rainfall on the hydromechanical behavior and stability of unsaturated lateritic slopes, commonly found in tropical regions. By employing both experimental and computational analyses, this research goes beyond traditional assumptions about soil behavior, providing an insight into the behavior of clayey and sandy lateritic soils in unsaturated condition. A probabilistic Monte Carlo analysis highlights the critical role of the variability of soil strength parameters on the assessment of slope stability. Detailed experimental design and computational modeling capture the complex interactions between hydraulic and mechanical soil behaviors, contributing substantial empirical data to geotechnical engineering fields. Notably, the shear strength prediction models adapted for unsaturated soils significantly influence slope behavior, demonstrating similar patterns in factor of safety reduction across different hydraulic models during rainwater infiltration. The analysis also confirmed hydraulic parameters with marked differences in porosity and water retention capacities between the soils impacting their susceptibility to saturation and shear strength reduction under similar conditions. This comprehensive approach not only advances our understanding of lateritic soils under changing climatic conditions but also enhances the predictive capabilities for slope stability, guiding effective risk management and engineering practices in tropical regions.

Keywords: Hydromechanical properties; Unsaturated lateritic soils; Slope stability; Monte Carlo simulation; Rainfall infiltration.

Resumo

As rupturas de taludes induzidas pela chuva representam riscos significativos e impactos econômicos em todo o mundo. Este estudo investiga o impacto da chuva no comportamento hidromecânico e na estabilidade de taludes lateríticos não saturados, comumente encontrados em regiões tropicais. Ao empregar análises experimentais e computacionais, esta pesquisa vai além das suposições tradicionais sobre o comportamento do solo, fornecendo uma visão sobre o comportamento de solos lateríticos argilosos e arenosos em condições não saturadas. Uma análise probabilística de Monte Carlo destaca o papel crítico da variabilidade dos parâmetros de resistência do solo na avaliação da estabilidade do talude. O projeto experimental detalhado e a modelagem computacional capturam as interações complexas entre os comportamentos hidráulicos e mecânicos do solo, contribuindo com dados empíricos substanciais para os campos da engenharia geotécnica. Notavelmente, os modelos de previsão da resistência ao cisalhamento adaptados para solos não saturados influenciam significativamente o comportamento do talude, demonstrando padrões semelhantes na redução do fator de segurança em diferentes modelos hidráulicos durante a infiltração da água da chuva. A análise também confirmou os parâmetros hidráulicos com diferenças marcantes na porosidade e nas capacidades de retenção de água entre os solos, afetando sua suscetibilidade à saturação e à redução da resistência ao cisalhamento em condições semelhantes. Essa abordagem abrangente não apenas amplia nossa compreensão dos solos lateríticos em condições climáticas variáveis, mas também aprimora as capacidades preditivas para a estabilidade de taludes, orientando práticas eficazes de gestão de riscos e engenharia em regiões tropicais.

Palavras-chave: Propriedades hidromecânicas; Solos lateríticos não saturados; Estabilidade de taludes; Simulações de Monte Carlo; Infiltração de água da chuva.

1. Introduction

Rainy seasons can lead to devastating slope failures, causing extensive material damage and loss of life. From 2004 to 2016, a total of 4,862 fatal landslides were recorded globally, resulting in 55,997 deaths (Zhou et al. 2021). In Italy, over 4,103 landslide-related fatalities were recorded from 1950 to 2008 (Salvati et

https://doi.org/10.5380/qeg.v17i1.101895

al. 2010). Indonesia is also affected by frequent landslides during its rainy season, with 569 incidents and 1,362 fatalities recorded between 1998 and 2007 (Allo et al. 2014). Since 1900, areas along China are also severely affected (Huang & Li 2011). In the United States of America, landslides imposed repair costs of about US$ 106 million annually to the state highway system, with total national expenses projections surpassing US$ 2 billion (Walkinshaw 1992, Klose et al. 2016).

Being a worldwide issue, slope failures also affect Brazil. Brusque, a city in the state of Santa Catarina, documented 500 landslides, while São Paulo's metropolitan area recorded 2,038 landslides in 2010 alone. Pernambuco state listed 3,138 landslides from 1988 to 2019 and Rio Grande do Sul state registered 16,862 mass movements in 2024 (Osako 2021, Abramento et al. 2022, Xavier et al. 2022, Mayumi et al. 2023, Andrades-Filho & Mexias 2024). These events are expected to become more frequent and severe in the context of climate change, which is projected to intensify precipitation patterns and increase the occurrence of extreme rainfall events globally (Comegma et al. 2013, Auflič et al. 2023, Koch et al. 2023, Pei et al. 2023). Studies such as Huaxiang et al. (2023) indicate that more frequent and intense rainfall could significantly affect landslide rates, particularly by increasing the risk of shallow failures during wet seasons. Understanding and predicting the hydromechanical response of slopes to rainfall is therefore of growing urgency, especially in tropical regions already susceptible to landslide hazards.

Understanding the hydromechanical behavior of unsaturated soils is crucial for soil mechanics-based stability analysis. The impact of rainwater infiltration on the soil's shear strength and hydraulic conductivity in the unsaturated zone is well documented and often predicted based on the soil-water characteristic curve (SWCC) (Fredlund et al. 2012, Karim et al. 2022). Consequently, the SWCC is essential for implementing mechanistic models in practice (Lu 2016, Guillaume et al. 2023), with models such as those proposed for van Genuchten (1980) model being widely adopted. More recently, Priesack & Durner (2006) extended the use of the SWCC to predict the hydraulic conductivity function for bimodal soils. These models, widely discussed in literature (Ghezzehei et al. 2007), necessitate careful consideration of "model selection uncertainty" during application (Li et al. 2019). There are also several tools for the in-situ determination of properties associated to the triggering of rainfall-induced landslides processes. For instance, tools like the Guelph Permeameter are instrumental in measuring field-saturated permeability and estimating unsaturated permeability through Gardner's (1958) empirical equation (Reynolds & Elrick 1986).

The shear strength of unsaturated soils is often found to be nonlinear (Zhang et al. 2014, Pande et al. 2021, Pham & Melis (2022), with Vanapalli et al. (1996) highlighting how shear strength changes can be estimated based on water content changes obtained from the SWCC. A prediction model that has been frequently used for tropical soils was proposed by Vilar (2006) based on a hyperbolic equation, allowing a straightforward approach (Patil et al. 2017).

Traditional slope stability analyses for circular slides typically employ a deterministic method based on Limit Equilibrium (LE) and Factor of Safety (FS) principles (Duncan et al. 2014) and geotechnical analysis software, often combining LE and Finite Element models for transient seepage analysis. Researchers have applied these types of software tools to investigate the effects of rainwater infiltration on the stability of unsaturated slopes, demonstrating their utility in various studies (e.g., Rahardjo et al. 2007, Yeh et al. 2015, Lin & Zhong 2019, Rahardjo et al. 2019, Augusto Filho & Fernandes 2019, Yu et al. 2020, Wang et al. 2020, Zhou et al. 2022). However, probabilistic approaches, such as the Monte Carlo Method, are becoming popular for its ease and adaptability (Fenton & Griffiths 2008, Huvaj & Oğuz 2018, Lu et al. 2022, Siacara et al. 2024), allowing a more detailed assessment of the role of the uncertainty of strength parameters on the likelihood of landslides (Nguyen & Likitlersuang 2019). In this context, a detailed assessment of statistical input parameters becomes of paramount importance. For instance, the correlation between cohesion (c') and the internal friction angle (ϕ') must be evaluated, as it is known to significantly influence the analysis results (Siacara et al. 2020).

The statistical evaluation of shear strength parameters for probabilistic analysis presents challenges due to the inherent limitations of testing methods. These investigations are costly and time-consuming. Therefore, employing simplified methods to derive mean values, standard deviations, and the cohesion-friction angle (c'-ϕ') correlation for local soils can prove beneficial to the implementation of probabilistic approaches. Furthermore, the unique texture and overall characteristics of lateritic soils can result in unexpected behavior. Comparative data and studies on the variability of soils with such pedological characteristics are scarce (Osinubi & Nwaiwu 2009, Sun et al. 2016, Miguel & Vilar 2009, Camapum de Carvalho & Gitirana Jr. 2021).

This study provides a detailed examination of how rainfall infiltration affects the hydromechanical properties and slope stability of two types of unsaturated lateritic soils – clayey and sandy – found in the in the south region of Brazil. By integrating data from both laboratory experiments and field observations with computational and statistical analyses, this paper offers new insights into the behavior of lateritic soils under wetting conditions. The findings contribute to the understanding of slope stability challenges in tropical soils and offer practical guidance for geotechnical engineering applications, particularly in regions with similar soil profiles. This work adds valuable knowledge to the field of Geotechnical Engineering, enhancing the predictive accuracy of slope stability models and informing effective landslide risk management strategies.

2. Study area

The soils investigated in this study are from the cities of Londrina and Mandaguaçu, situated in the state of Paraná, in the southern region of Brazil (Fig. 1). Table 1 outlines the climatic characteristics of these cities. The prevailing climatic conditions in these areas significantly influence the pedogenesis of tropical soils, characterized by intense weathering processes (Almeida et al. 2011, Gidigasu 1976).

In geological terms, Londrina region is predominantly underlain by basaltic volcanic rocks of the Serra Geral Group. This volcanic sequence comprises multiple lava flows with distinct lithological and geochemical characteristics, which may be reflected in different weathering profiles (Gomes et al. 2018, Licht & Arioli 2020). In Londrina region, above the bedrock lies a residual horizon averaging 10 meters in thickness, with varying degrees of weathering along the soil depth (Cavalcante et al. 2007). The municipality of Mandaguaçu falls within the Goio-Erê Formation, part of the Caiuá Group. This formation primarily consists of quartzose sandstones and features erosive and abrupt contacts with the basalts of the Serra Geral Group (Sá et al. 2021). Figure 2 shows the geological map of the study area.

Table 1: Range of the average climatic characteristics of Londrina and Mandaguaçu (Nitsche et al. 2019 – adapted).

Characteristics		Location	
		Londrina	**Mandaguaçu**
Köppen Climate Classification		Cfa	Cfa
P (mm)	Annual	1600-1800	1400-1600
	Summer	500-600	500-600
	Winter	200-300	200-300
T (ºC)	Annual	21-22	22-23
	Summer	24-25	25-26
	Winter	17-18	18-19
P-PET (mm)	Annual	600-700	500-600
	Summer	200-250	150-200
	Winter	50-100	50-100

Note: P = Precipitation. T = Temperature. P-PET = Precipitation minus Potential Evapotranspiration. Summer coincides with the wet season while winter aligns with the dry season.

The soils of Serra Geral Formation in the Londrina region exhibit a structure highly porous and, in some instances, may be metastable, exhibiting collapsible behavior (Christoni et al. 2019, Zanin et al. 2021, Fredlund et al. 2012, p. 33). The soil in Londrina is classified using the MCT (Miniature, Compacted, and Tropical) system developed by Nogami & Villibor (1980) as lateritic clayey soil, while the soil in Mandaguaçu is identified as lateritic sandy soil.

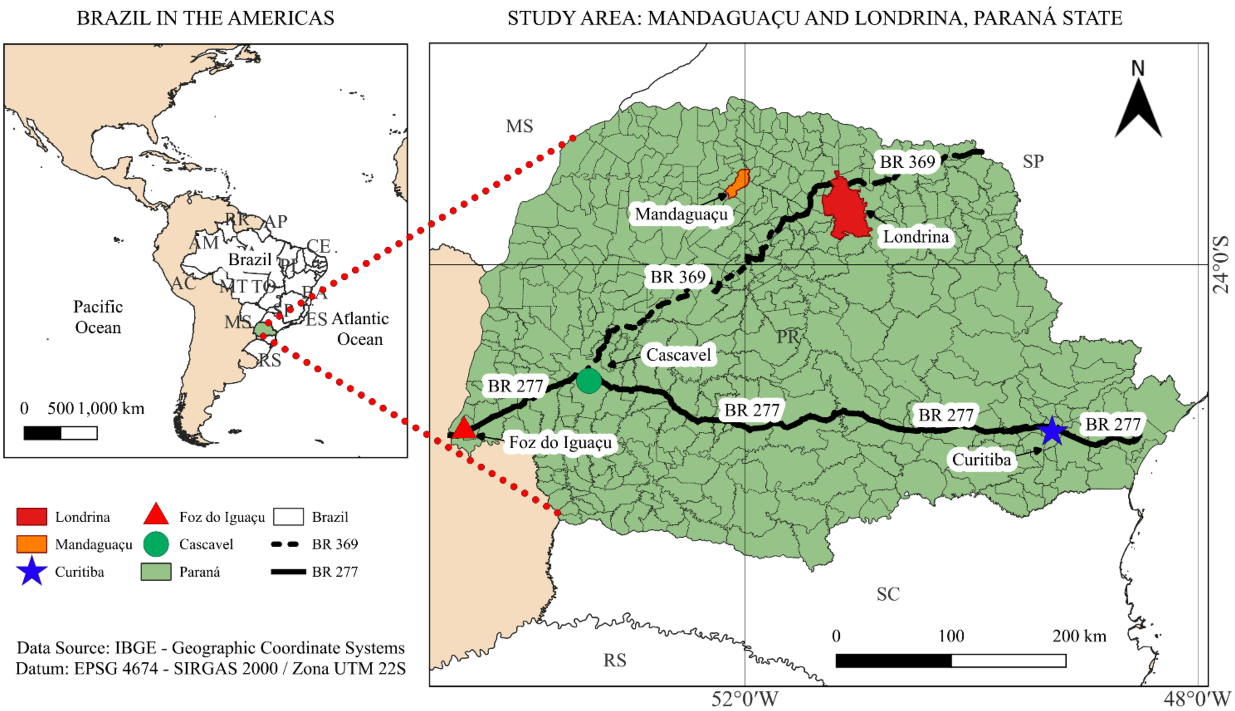

Figure 1: Study area location.

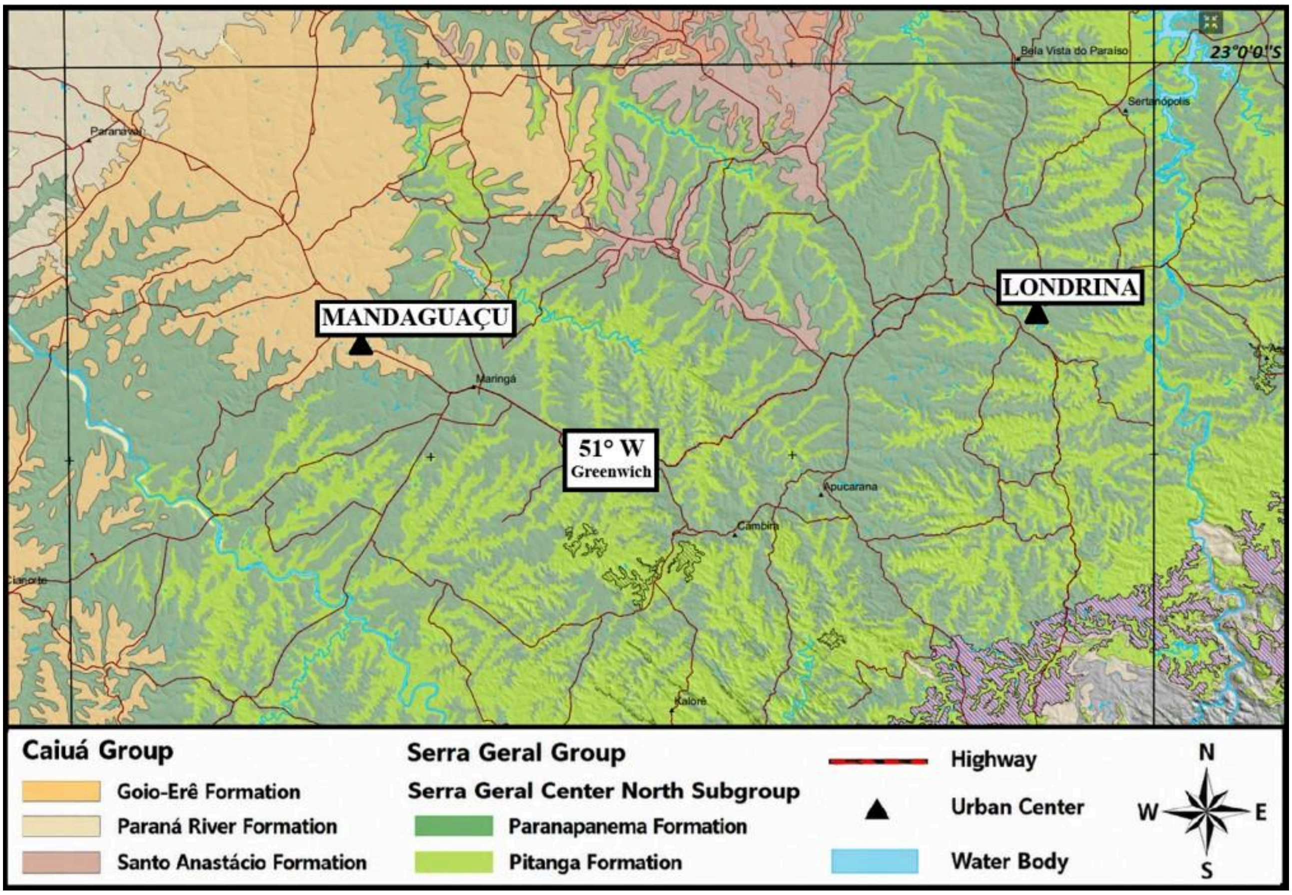

Figure 2: Geological map of the region, northern Paraná State, Brazil, showing the locations of Londrina and Mandaguaçu cities. Adapted from Licht and Arioli (2018).

The studied lateritic soils were formed through advanced weathering and laterization processes acting on volcanic and sedimentary parent materials under humid climatic conditions. These soils are typically characterized by iron and aluminum oxide enrichment, microaggregated structure, and predominance of kaolinite in the clay fraction (Oliveira et al., 2022). Additional information regarding particle-size distribution, physical indexes, and lateritic soil structure of the studied materials is presented in Table 2 and discussed in detail by Oliveira et al. (2022), including the influence of macro and microporosity on the hydraulic behavior of these soils. Table 2 outlines the characterization and average index properties of these soils, from samples collected in a range of 2 meters depth.

Table 2 – Physical characterization of soils from Londrina and Mandaguaçu, from Oliveira et al. (2022).

Property	Londrina Lateritic Clay (LC)	Mandaguaçu Lateritic Sand (LS)
*Sand (%)	21	71
*Silt (%)	23.5	15.5
*Clay (%)	55.5	13.5
**Sand (%)	20	84
**Silt (%)	77.5	16
**Clay (%)	2.5	0
Natural Water content, w (%)	32	12
Liquid limit, w_L (%)	51	31
Plastic limit, w_P (%)	38	15
Plasticity index (%)	13	16
Particle density, ρ_s (g/cm³)	3.03	2.69
Void ratio, e	1.7	0.7
Porosity, n (%)	63	41
Natural Dry density, ρ_d (g/cm³)	1.12	1.59

Note: *Particle size distribution with deflocculant – ABNT (1995) and ASTM (2017). ** Particle size distribution without deflocculant – ABNT (1995) and ASTM (2017).

3. Materials and Methods

The research program was structured in two parts. The first covers the experimental characterization of the soils through field and laboratory testing, producing the input data for the numerical models. The second comprises the design and implementation of the computational models and the analyses performed. The methodological sequence is presented as follows:

a) Experimental Program

- Identification of study sites: Londrina – lateritic clay (LC) and Mandaguaçu – lateritic sand (LS), northern Paraná, Brazil; soil parameters from existing literature were used to complement field and laboratory data.
- Undisturbed soil sampling for laboratory testing. Field investigations and soil sampling were performed at the same locations in each area.
- Determination of the SWCC.
- Determination of saturated hydraulic conductivity by Guelph permeameter field tests, with statistical treatment of results.
- Determination of the unsaturated hydraulic conductivity function.
- Direct shear tests under flooded and air-dried conditions, including statistical analysis of strength parameters and prediction of the unsaturated shear strength envelope.

b) Numerical Modeling

- Definition of representative hypothetical slope geometry, initial pore water pressure conditions, and design rainfall event.
- Definition of two hydraulic models with distinct unsaturated hydraulic conductivity functions, MOD1 (Priesack & Durner, 2006) and MOD2 (Gardner, 1958), applied to both soils, resulting in four numerical models.
- Transient flow analyses in SEEP/W (GeoStudio, 2020a) to simulate rainfall infiltration and obtain pore water pressure distributions over time.
- Deterministic slope stability analyses in SLOPE/W (GeoStudio, 2020b), with determination of the minimum Factor of Safety throughout the rainfall event duration.
- Complementary probabilistic slope stability analysis via Monte Carlo method in SLOPE/W (GeoStudio, 2020b), to assess the influence of shear strength parameter variability.

3.1. Hydraulic behavior parameter determination methods

a) Determination of the soil-water characteristic curve:

The filter paper method was used for the determination of the SWCC of the materials along wetting and drying paths. The testing procedure adhered to the guidelines set by ASTM D5298-16 and Marinho & Oliveira (2006), utilizing Whatman 42 filter paper. The calibration equations proposed by Chandler et al. (1992) were adopted for this purpose:

For $w_p \leq 47\%$:

$$\Psi_p \text{ (kPa)} = 10^{(4.84 - 0.0622\, w_p)}\ \% \quad (1)$$

For $w_p > 47\%$:

$$\Psi_p \text{ (kPa)} = 10^{(6.05 - 2.48\, \log w_p)}\ \% \quad (2)$$

where: Ψ_p is the suction of the filter paper; and w_p is the volumetric moisture content of the filter paper.

In this study, both the LC and LS soils were analyzed along drying and wetting paths to define their soil-water retention behavior of undisturbed soil samples. For the LC soil, the drying path was obtained from Oliveira et al. (2022) using filter paper and pressure plate tests, while the wetting path was obtained by Oliveira (2023) using the filter paper method. For the LS soil, the drying path data were obtained from Oliveira et al. (2022) using filter paper and pressure plate tests, whereas the wetting path was determined in the present study using the filter paper method. The combination of filter paper and pressure plate technique allows a more comprehensive characterization of the soil-water retention curve over a wider suction range, since these methods are complementary.

Although the drying and wetting curves were obtained at different moments, they were considered representative of the hydraulic behavior of the soils and were combined to define the complete retention curves. All tests were performed on undisturbed soil samples, and the consistency between specimens obtained at different stages was verified based on their physical index properties.

The SWCC were fitted using the bimodal equation proposed by Gitirana Jr. & Fredlund (2004):

$$S = \frac{S_1 - S_2}{1 + \left(\frac{\Psi}{\sqrt{\Psi_{b1}\Psi_{res1}}}\right)^{d_1}} + \frac{S_2 - S_3}{1 + \left(\frac{\Psi}{\sqrt{\Psi_{b2}\Psi_{res1}}}\right)^{d_2}} + \frac{S_3 - S_4}{1 + \left(\frac{\Psi}{\sqrt{\Psi_{b2}\Psi_{res2}}}\right)^{d_3}} + S_4 \quad (3)$$

where: S, S_1 and S_2 are degrees of saturation but can also be treated as volumetric moisture contents; Ψ, Ψ_b and Ψ_{res} represent suction levels; and *d* is *a* curve-smoothing parameter.

Furthermore, the SWCC was also refined by Durner (1994) model in equation (4), with parameters manually adjusted for optimal alignment.

$$S = w_1\left[\frac{1}{1 + (\alpha_1|\Psi|)^{n_1}}\right]^{m_1} + w_2\left[\frac{1}{1 + (\alpha_2|\Psi|)^{n_2}}\right]^{m_2} \quad (4)$$

where: w_2=(1-w1); m_1=(1-(1/n_1)); and m_2=(1-(1/n_2)).

The curves obtained from the regression analyses using the Gitirana Jr. & Fredlund (2004) model was used in the numerical simulations. The curve established using Durner (1994) model was employed to obtain the parameters for the Priesack & Durner (2006) unsaturated hydraulic conductivity model.

b) Permeability

The permeability of the soils found in the study areas was measured using the Guelph Permeameter. A total of 21 tests were conducted in LC and 15 in LS, utilizing the Guelph Permeameter model 2800, Figure 3.

The boreholes were drilled to depths of 50 to 70 cm, with a diameter of 6 cm, spaced at least 2 m apart. The tests commenced under the soil's natural moisture conditions, with water head heights of 5 and 10 cm applied.

The field-saturated permeability coefficient (k_{fs}), the matric potential of flow (φ_{Gm}) and the parameter (α_{gp}) were calculated using the method proposed by Reynolds & Elrick (1986), as follows:

$$Q_{gp_1} = \left(\frac{2\pi H_{gp_1}^{\ 2}}{C_1} + \pi a^2\right) k_{fs} + \left(\frac{2\pi H_{gp_1}}{C_1}\right) \varphi_{Gm} \quad (5)$$

$$Q_{gp_2} = \left(\frac{2\pi H_{gp_2}^{\ 2}}{C_2} + \pi a^2\right) k_{fs} + \left(\frac{2\pi H_{gp_2}}{C_2}\right) \varphi_{Gm} \quad (6)$$

$$\alpha_{gp} = \frac{k_{fs}}{\varphi_{Gm}} \quad (7)$$

where: Q_{gp} is the steady-state flow rate; H_{gp} is the water head height; a is borehole radius; C_1 and C_2 are the shape factor, which depends on the soil type and the $\frac{H_{gp}}{a}$ ratio; and α_{gp} as defined in Equation (7).

The α_{gp} parameter was initially estimated at 0.12 cm^{-1}, and the C_1 and C_2 values were derived from the equations provided by Zhang et al. (1998).

Regarding the variables k_{fs} and α_{gp}, statistical analyses including the Shapiro-Wilk normality test, as well as determinations of mean, variance, standard deviation, and probability density function were executed. The formulation of unsaturated hydraulic conductivity curves was achieved through the application of two distinct methodologies: the approaches developed by Priesack & Durner (2006) and Gardner (1958). This research utilized the average k_{fs}, across both models for the analysis.

3.2. Determination of Resistance Parameters

Direct shear tests were conducted under both flooded and air-dry conditions, following ASTM D3080-11 standards with a conventional direct shear apparatus. Undisturbed soil specimens measured 60 mm in width and length, and 20 mm in height. In total, 48 tests were carried out, divided equally between two soil types. Specifically, 16 tests were performed under flooded conditions and 8 under air-dry conditions, grouped into sets of four specimens, establishing 12 shear envelopes. The normal total stresses applied were 50, 100, 200, and 300 kPa, representing stress levels compatible with the field conditions analyzed in this study. The shear displacement rate was 0.095 mm/min, with a maximum relative horizontal displacement of 6 mm.

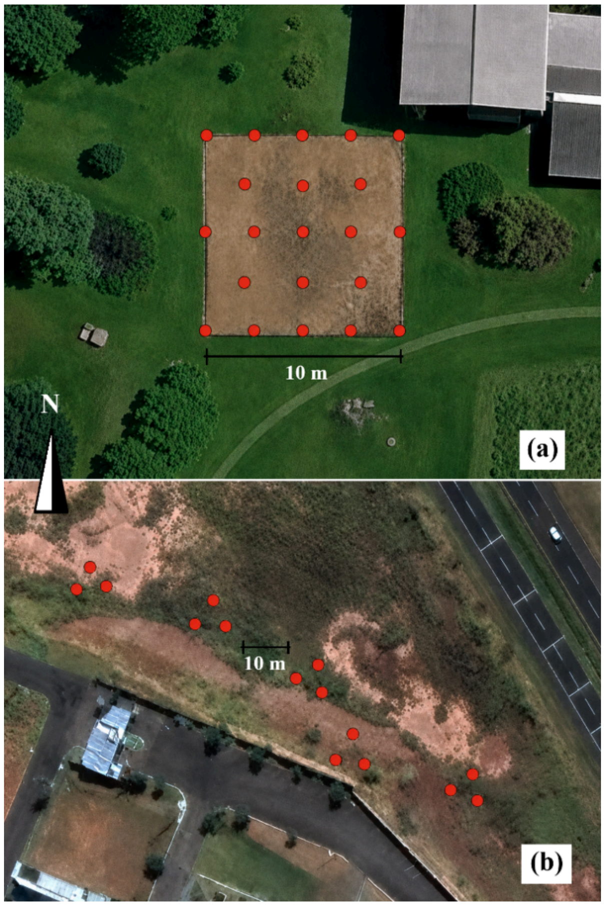

Figure 3: Guelph permeameter tests location. (a) LC (b) LS.

The flooded specimen tests aimed to assess statistically the saturated shear strength parameters. The failure stress-state dataset (i.e., the pairs of normal and shear stresses) underwent combinatorial analysis to produce 256 envelopes per soil, following the procedures developed by Di Matteo et al. (2013). Linear regression was used to determine these envelopes, from which c', ϕ' and tan ϕ' were calculated. These variables underwent descriptive statistical analysis, including probability density function evaluation and correlation coefficient calculation between c' and ϕ'.

Conversely, the air-dry tests aimed to determine the ultimate unsaturated resistance values, employing Vilar (2006) method. For these tests, specimens were stored in a dry, cool, and sun-protected environment, with the drying process extending until moisture content was constant.

Building on this, an analysis was carried out to compare the predicted shear strength envelopes for the unsaturated soils obtained using the Vanapalli et al. (1996) and Vilar (2006) models. Unlike the linear increase in shear strength with suction commonly associated with the ϕ^b (rate of shear strength increase with matric suction) parameter in the extended Mohr-Coulomb criterion proposed by Fredlund et al. (1978), these models allow a nonlinear representation of the contribution of matric suction to shear strength, and are respectively presented as:

$$c_{ap} = c' + (u_a - u_w)\left[(tan\phi')\left(\frac{\theta_w - \theta_r}{\theta_s - \theta_r}\right)\right] \quad (8)$$

$$c_{ap} = c' + \frac{u_a - u_w}{a + b(u_a - u_w)} \quad (9)$$

where: c_{ap} is the apparent cohesion of the unsaturated soil; c' is the effective cohesion intercept; $(u_a$-$u_w)$ is the matric suction of the soil on the failure plane; ϕ' is the effective friction angle; θ_w is the volumetric water content; θ_r is the residual volumetric water content; θ_s is the saturated volumetric water content; a and b are curve-fitting parameters, $a = \frac{1}{tan\phi'}$; $b = \frac{1}{(c_{max} - c')} - \frac{a}{(u_a - u_w)}$; and c_{max} is the maximum measured cohesion, determined under air-dried conditions.

3.3. Computational Analysis Methods and Models for Slope Stability

The study was designed to enable analyses of slope response under varied loading and environmental conditions. For this purpose, the GeoStudio (2020a, 2020b) software suite was utilized. The study was carried out on theoretical slope models whose geometry is illustrated in Figure 4. The soil profile was considered homogeneous and isotropic, with the initial groundwater level set at 5 meters below the base of the slopes.

The definition of the initial pore pressure distribution is dependent on antecedent atmospheric conditions. The initial pore pressures were defined according to the work of Oliveira (2023). The author conducted in situ measurements with tensiometers in LC over the years 2020 to 2021, at depths of 0.50 m, 0.75 m, and 1.00 m. This scenario was assumed to reflect summer/wet climate conditions. The initial distribution for the analysis is presented in Figure 5.

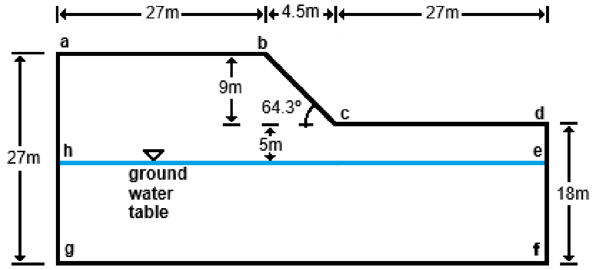

Figure 4: Geometry and analysis domain (modified from Rahardjo et al. 2007). Note: a, b, c, d, e, f, g, h = geometric definition points.

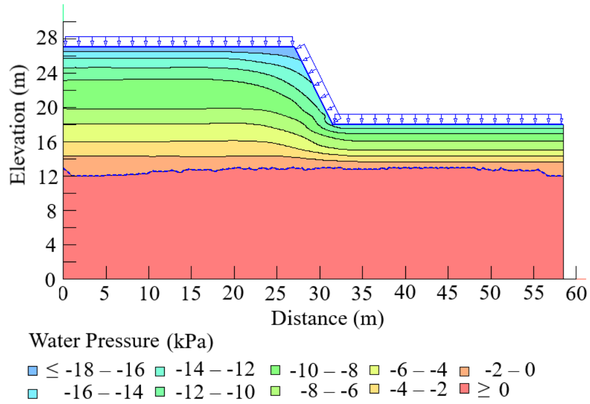

Figure 5: Initial distribution of pore-water pressures based on the initial pore-pressure data obtained by Oliveira (2023).

A representative rainfall event was used to investigate the effects of weather conditions, similar to those approaches adopted by Ng et al. (2001) and Zeng et al. (2017). The design rainfall scenario adopted in this study was defined according to the Huff (1967) method for the fourth quartile with 50% probability, considering rainfall events lasting longer than 24 hours. Based on the regional IDF equation and its parameters, the method defines the rainfall intensity, temporal distribution, and total accumulated precipitation for the selected location. In order to evaluate the representativeness of the adopted rainfall scenario, the rainfall obtained through the Huff method was compared with historical accumulated daily rainfall records obtained from Hydrological Information System (IAT, 2021) monitoring data. The comparison indicated that the adopted rainfall scenario is consistent with historically observed rainfall events in terms of both precipitation distribution and accumulated volume. The rainfall scenario adopted for the numerical analyses corresponded to the design rainfall calculated for LC, which presented the highest accumulated precipitation among the evaluated conditions. This rainfall event was selected as a representative and conservative scenario for application to both studied soils, and the resulting rainfall distribution is presented in Figure 6.

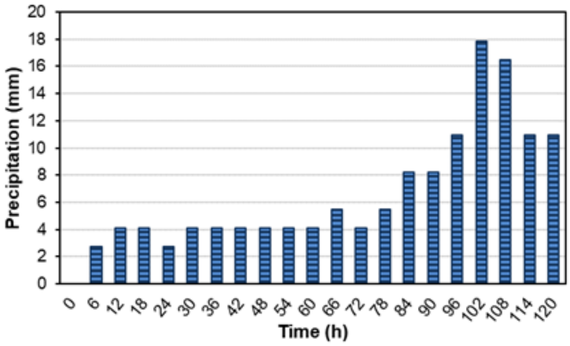

Figure 6: Design rainfall obtained using the Huff (1967) method and validated against historical rainfall records from IAP monitoring data.

3.4. Analyzed Scenarios

Two models, MOD1 and MOD2, were developed featuring distinct unsaturated hydraulic properties. The models are structured to analyze infiltration using different parameterizations of hydraulic properties derived from various sources and methodologies.

MOD1 is based on saturated permeability coefficients (k_{fs}) obtained using the Guelph Permeameter, unsaturated hydraulic conductivity curves (k_{fsPD}) obtained using the Priesack & Durner (2006) model, and SWCCs ($f_{GF}\theta(\psi)$) obtained by using methodologies developed by Gitirana Jr. & Fredlund (2004).

MOD2, on the other hand, adopts similar methodologies but integrates different parameter estimations for unsaturated hydraulic conductivity. This model uses initial k_{fs} values from the Guelph Permeameter and refines the conductivity curves and characteristic curves using α_{gp}, as described in equation (7), and Gardner (1958) models based on experimental data and theoretical formulations to obtain the unsaturated hydraulic curve ($k_{fsG}(\psi)$).

Both MOD1 and MOD2 models utilize a combination of empirical data, field measurements such as those from tensiometers (Oliveira, 2023), and theoretical models to establish a robust framework for analyzing water movement through unsaturated soil systems. The approaches provide a comprehensive view of how each model behaves under simulated conditions reflecting realistic environmental scenarios, such as varying soil moisture levels and hydraulic pressures.

3.5. Seepage and Slope Stability Analyses

The SEEP/W 2018 (GeoSlope, 2020a) package allows flow analyses in unsaturated soils using the finite element method, enabling the determination of pore-water pressure distributions within the soil mass under rainfall infiltration conditions and considering the hydraulic properties of unsaturated soils. In the analysis, a 5-day rainfall event (design rainfall) was considered, followed by an additional 2-day period without precipitation, resulting in a total simulation period of 7 days. The SEEP/W (GeoSlope, 2020a) analysis was performed under transient conditions using 84 time steps with a linear time increment of 0.083333 day (2 hours), while results were saved every 2 steps (4 hours). The initial pore-water pressure distribution was assigned through a spatial function based on a kriged surface. The finite element mesh used in the transient seepage simulation was a hybrid type (i.e., 2D quadrilateral and triangular elements), with dimensions ranging from 0.1 m near the surface to 1 m at greater depths. Linear elements were utilized, totaling 25,642 nodes and 25,377 elements.

The Bishop (1955) limit equilibrium method was employed to compute FS values. A slope stability analysis was conducted every 4 hours, from day 0 to day 7. It is not feasible to directly apply the shear strength envelope from Vilar (2006) in the SLOPE/W 2018 software (GeoSlope, 2020b). Therefore, a strategy was developed for implementation using the equations from Vanapalli et al. (1996) along with an equivalent SWCC that would produce an apparent cohesion identical to that predicted using the Villar (2006) model.

3.6. Monte Carlo Simulations

Monte Carlo probabilistic analyses were performed using the native probabilistic analysis module available in SLOPE/W considering the state of the slope after the end of a seven-day atmospheric event. The same parameters and conditions from the deterministic analysis were used. The probabilistic analyses were conducted considering independently distributed random variables for the shear strength parameters c' and ϕ', based on the defined probability density functions and without spatial correlation between variables. The probability density function of c' and ϕ', were truncated at the maximum and minimum values obtained in the combinations, to avoid unacceptable negative values in solutions by Monte Carlo Simulation (Siacara et al. 2020).

The number of simulations was set at 5,000, allowing reasonable computation times and still providing sufficiently accurate results. This number of simulations is consistent with that adopted in other studies, such as Nguyen and Likitlersuang (2019).

4. Results and Discussion

4.1. Soil-Water Characteristic Curve

Figure 7 displays the obtained soil-water characteristic curves and Table 3 lists their corresponding best-fit parameters. The SWCC of the soil from LC presents significant hysteresis, while the soil from LS exhibits virtually no hysteresis. This observation coincides with the findings of Malaya & Sreedeep (2012), who noted a tendency for less hysteresis in coarse soils compared to fine collapsible soils. The almost complete absence of hysteresis was also identified by Fernandes (2016) and Augusto Filho & Fernandes (2019) in a study of a similar Brazilian residual tropical sand. The models have shown good fit for tropical soils and high accuracy in fitting bimodal SWCCs of tropical soils.

The volumetric moisture content of LC is at least 50% higher than that of LS across the entire suction range. The air-entry values of both soils are similar, around 2 kPa. The slopes of the desaturation lines for the macropores are also quite similar, decreasing at a rate of approximately 2 cm^3/cm^3 for each 1 kPa increase in suction.

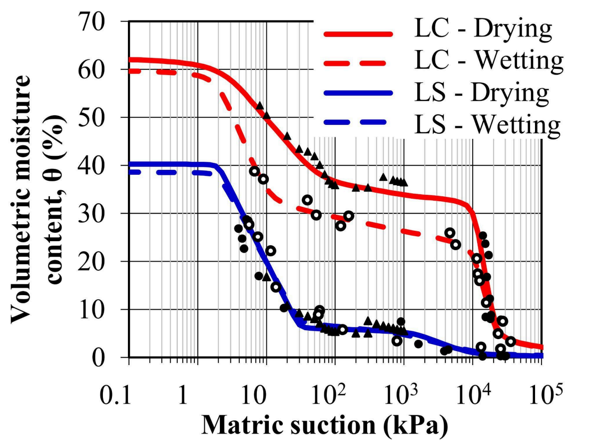

Figure 7: Drying and wetting SWCC from LC and LS fitted with Gitirana Jr. & Fredlund (2004) model. Note: Symbol shape indicates the test method. Circles: filter paper. Triangles: pressure plate. Symbol fill indicates the hydraulic path. Filled: drying. Open: wetting. LC and LS drying data from Oliveira et al. (2022); LC wetting data from Oliveira (2023); LS wetting data from this study.

The residual volumetric moisture content of the macropores is defined at similar suctions, with 10 kPa for LC and 30 kPa for LS. This slight difference may be related to the larger volume of inter-aggregate pores in LS, as per Oliveira et al. (2022). It is in this region where the greatest differences in volumetric moisture content between the soils occur, with values for LC being more than twice as high as those for LS.

The most pronounced difference between the curves occurs in the desaturation zone of the micropores, caused by the larger volume of micropores in LC compared to LS. Generally, these behaviors are close to what would be expected for the studied soils, which are tropical (Camapum de Carvalho & Gitirana Jr 2021).

The curves determined using Durner (1994) model are similar to the curves from the model by Gitirana Jr. & Fredlund (2004). The coefficients of determination of the Gitirana Jr. & Fredlund (2004) model applied to the data for the soils from LC and LS are 0.9841 and 0.9507, respectively. The coefficients of determination of the Durner (1994) model applied to the soils from LC and LS are 0.9864 and 0.9674, respectively.

4.2. Guelph Permeameter

A lognormal distribution for k_{fs} and α_{gp} was identified based on the p-value results from the Shapiro-Wilk test on valid and transformed data. This distribution is characterized by the property that the logarithms of the values follow a normal distribution. Valid data were considered those from tests where no calculated variables (k_{fs} or α_{gp}) resulted in negative values. Outliers were identified and removed from the analysis using the interquartile range method and Full Normal Plot. Table 4 presents the statistical parameters obtained, considering the lognormal distribution, as per Koch & Link (2002).

Table 3: Fitting parameters for the wetting SWCCs.

	Soil	
	LC	**LS**
Fitting by Gitirana Jr. & Fredlund (2004)		
θsat (%)	60	39
ΨVEA1 (kPa)	2	2
Ψres1 (kPa)	10	30
θres1 (%)	52	18
ΨVEA2 (kPa)	11000	1400
θb (%)	40	14
Ψres2 (kPa)	20000	8700
θres2 (%)	5	1
α	0.07	0.03
R^2	0.984	0.951
Fitting by Durner (1994)		
θs (%)	60	39
θr (%)	1.05	0.85
w1	0.562	0.875
α1 (cm^{-1})	0.313	0.185
n1	2.0	2.3
α2 (cm^{-1})	0.000087	0.0010
n2	3.05	2.005
R^2	0.986	0.967

The average k_{fs} values for LC and LS were consistent with the saturated permeability values obtained in other tests and studies conducted in the same region, as reported by Teixeira & Pinese (2006), Souza & Celligoi (2011), and Rodriguez et al. (2015) for LC, and Fink (2018) for LS. Feki et al. (2020) highlights that field tests generally exhibit lower permeability values compared to laboratory tests, and such results may be related to air entrapment during the wetting process.

Table 4: Statistical parameters of k_{fs} and α_{gp}.

		Soil	
		LC	LS
		k_{fs}	
Mean	(cm/s)	$2.33 \cdot 10^{-4}$	$2.69 \cdot 10^{-4}$
Var.	(cm/s)²	$4.15 \cdot 10^{-8}$	$6.36 \cdot 10^{-8}$
SD	(cm/s)	$2.04 \cdot 10^{-4}$	$2.52 \cdot 10^{-4}$
CoV		0.87	0.94
		α_{gp}	
Mean	(cm^{-1})	0.114	0.037
Var.	$(cm^{-1})^2$	0.0091	0.0028
SD	(cm^{-1})	0.096	0.053
CoV		0.84	1.43

Note: Var. = variance; SD = standard deviation; CoV = coefficient of variation.

Additionally, the potential formation of a smeared layer during the drilling of boreholes for the Guelph Permeameter tests could influence results, particularly for the soil of LC, although the borehole walls were scarified using the standard bristle brush provided with the equipment. Reynolds (2008) and Rienzner & Gandolfi (2014) discuss extra precautions that can be taken concerning testing procedures.

The field-saturated permeability coefficients obtained for LC and LS are similar, in the order of 10^{-4} cm/s. Initially, one might expect that clayey soils would have lower permeability than sandy materials. However, the macropores of LC contribute to a permeability coefficient much higher than expected. At the same time, the relatively small clay fraction in LS's soil may still contribute to a slight reduction in the permeability coefficient. Therefore, the similar saturated permeability values observed can be explained by the bimodal pore-size distribution with macro and micropores characteristic of mature tropical lateritic soils (Oliveira et al., 2022).

The coefficients of variation (CoV) for k_{fs} and α_{gp} are high, around 100%, indicating significant variability in the hydraulic properties of the studied soils. Nielsen et al. (1973) and Duncan (2000) report CoV values between 68 and 90% for saturated permeability; Nielsen et al. (1973) and Benson et al. (1999) report values between 130 and 240% for unsaturated permeability. LS exhibits higher variation coefficients compared to LC, which is an expected result, as deduced from Gitirana Jr. & Fredlund (2016). Other statistical results of saturated hydraulic conductivity of Brazilian lateritic soils can be seen in Souza et al. (2022). The mean values (log-normal distribution) for k_{fs} and α_{gp} were adopted for the calculation of the unsaturated hydraulic conductivity functions.

4.3. Hydraulic Conductivity Curve

Figure 8 displays the unsaturated hydraulic conductivity curves for the two studied soils, estimated using the methods proposed by Priesack & Durner (2006) and Gardner (1958). The greatest discrepancies arise from the bimodality and are most significant at suctions above 100 kPa, a range not addressed by the computational simulations, neither measured in field. Additionally, it is worth noting the existence of a minimum permeability coefficient, as discussed by Ebrahimi-B et al. (2004), which was not necessary to impose in the SEEP/W (GeoStudio, 2020a) modeling performed in this study. However, for analyses involving higher suction ranges, this minimum value should be considered.

The permeability values obtained using the Gardner (1958) model for LS are consistently higher compared to the values for LC. The soil permeability of LS is greater than that of LC up to 30 kPa suction for all models. Beyond 30 kPa suction, the Priesack & Durner (2006) model for LC's soil predicts higher soil permeability compared to the Gardner (1958) model for LS.

4.4. Direct Shear Tests

4.4.1. Tests on Flooded Specimens

Figure 9 displays the dispersion of data points and the linear regression line adopted as corresponding to the shear strength envelopes. Figure 10 displays the histograms and distribution for c' and ϕ'. The descriptive statistics results for the parameters c', ϕ', and tan ϕ' obtained are listed in Table 5.

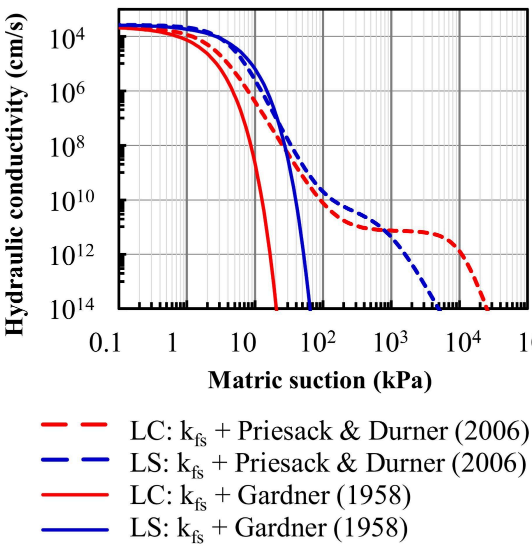

Figure 8: Unsaturated hydraulic conductivity functions of the soils from LC and LS.

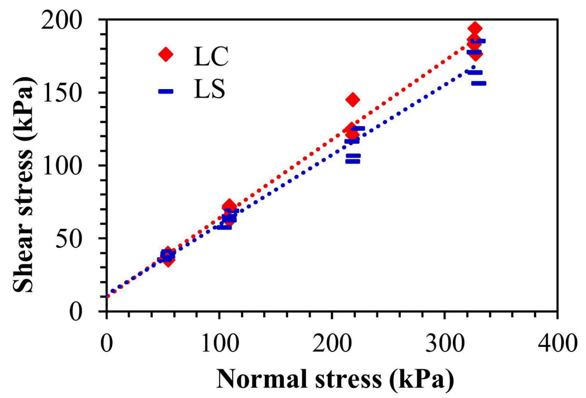

Figure 9: Shear strength envelopes for flooded specimens.

The average values of the analyzed parameters – c', ϕ', and tan ϕ' – correspond to those obtained from the best-fit envelop. In terms of effective cohesion, LS exhibits a greater range of values, while LC has the lowest minimum and LS the highest maximum values.

The standard deviation of effective cohesion found for LS is slightly higher, indicating a greater deviation from the central tendency. The coefficient of variation found for LC was 35% and for LS was 39%. These values are compatible with those determined in other studies, see Gitirana Jr & Fredlund (2016).

Regarding the effective friction angle, LC shows higher minimum and maximum values, with its minimum value only 2.3 degrees lower than the maximum value of LS. LS, despite being a sandy soil, exhibited an average effective friction angle of 25.6 degrees, which is lower than that presented by the clayey soil of LC, with a difference of 2.7 degrees. Oliveira et al. (2018) found a friction angle of 26.2 degrees in a triaxial test with an undisturbed soil sample from LS, which is compatible with that determined in this study. The standard deviation and coefficient of variation for ϕ' were considered within expected ranges for both soils. Duncan et al. (2014) reports typical values between 2 and 13%.

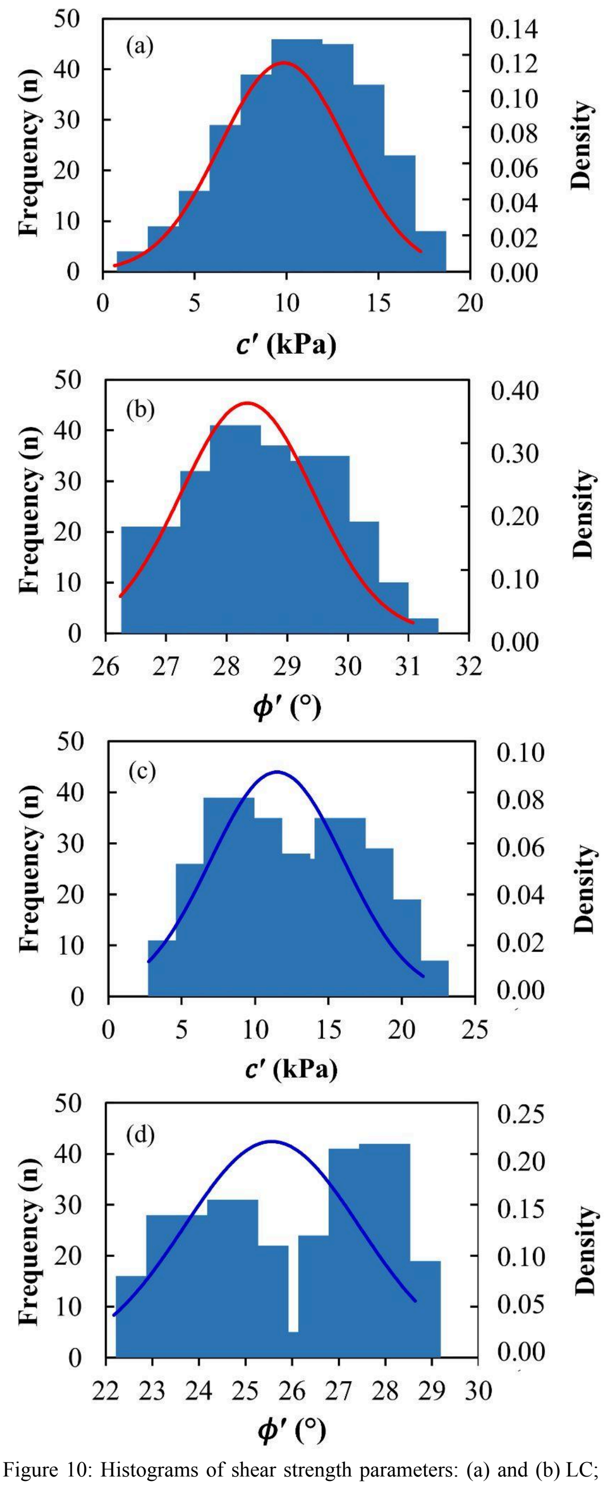

Figure 10: Histograms of shear strength parameters: (a) and (b) LC; (c) and (d) LS.

Table 5 – Statistical parameters of flooded shear data.

	LC	LS
	c'	
Min – Max (kPa)	0.5 – 17.3	2.6 – 21.5
Mean (kPa)	9.8	11.5
SD (kPa)	3.45	4.54
CoV	0.35	0.39
	ϕ'	
Min – Max (º)	26.2 – 31.1	22.1 – 28.6
Mean (º)	28.3	25.6
SD (º)	1.10	1.88
CoV	0.04	0.08
	tan ϕ'	
Min – Max	0.492 – 0.603	0.406 – 0.546
Mean	0.540	0.479
SD	0.025	0.040
CoV	0.05	0.08

Note: SD = Standard deviation; CoV = Coefficient of variation.

Figure 11 shows the dispersion of the ordered pairs of the parameters *c′* and ϕ' obtained from the shear strength envelopes, to better understand the local variability of the data. Each *c′*-ϕ' pair was obtained from an individual shear strength envelope generated through the combinatorial analysis procedure described previously, resulting in 256 envelopes for each soil. The dispersion of *c′*-ϕ' pairs, histograms, and the probability density function follow a normal distribution for *c′* and ϕ'. Notably, there is a lesser presence of points in the central region of LS's point cloud. This characteristic can also be observed in the histograms and the probability density function. In particular, the LS data suggest a tendency toward bimodal behavior, with a lower concentration of values around the central region and two preferential ranges of occurrence. This aspect may have been influenced by differences related to the samples used, the pre-consolidation stress, the natural heterogeneity of the soil, and even some degree of anisotropy resulting from the features of the original sedimentary rock. Further research is needed.

It is possible that this dispersion found is representative of the mechanical behavior for this soil. A similar distribution was found by Soulie et al. (1990) in assessing the variability of undrained strength of a clay, based on Vane Test trials, and by strength data from studies reported in Wu (2015). Correlations between effective cohesion and effective friction angle was -0.7272 (R^2 = 0.5288) for LC and -0.9002 (R^2 = 0.8104) for LS.

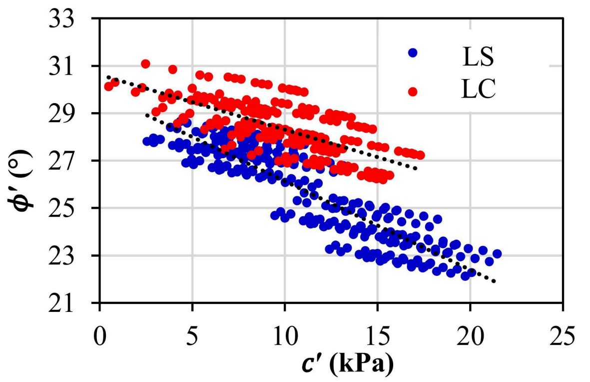

Figure 11: Dispersion plot for *c′* and ϕ' for the soils from LC and LS.

Greco (2016) provides an extensive evaluation of the variability and correlation of soil strength parameters, obtained from direct shear tests. The authors conclude that, generally, the correlation between strength parameters is predominantly negative, and the coefficients of variation are strongly affected by the sample size.

Di Matteo et al. (2013) and Branco et al. (2014) found *c′*-ϕ' correlations of -0.925 and -0.9, respectively, values close to those found for LS in this study, indicating a strong negative correlation. Cherubini (2000) notes that *c′*-ϕ' correlation values are usually between -0.5 and -0.75. The value determined for LC was -0.727, also considered a strong negative correlation. The range between -0.5 and -0.7 marks moderate negative correlation.

Di Matteo et al. (2013) and Di Matteo et al. (2015) performed a methodological approach and statistical analysis very similar to the proposal in this study for conducting flooded direct shear tests. The tests were combined into 256 *c′*-ϕ' pairs in alluvial fine-grained compacted samples. Wang & Akeju (2016) proposed an approach to characterize the distribution of *c′* and ϕ' and to quantify the *c′*-ϕ' correlation of the soil. The authors used data from Di Matteo et al. (2013), generated statistical models with n = 10,000. The results indicate that the application of the proposed model allows good estimates of the *c′*-ϕ' correlation of a specific soil with about only 10 *c′*-ϕ' pairs. Strong negative correlations of *c′*-ϕ' are also found in probabilistic studies of back analysis, for example, Liu et al. (2023).

4.4.2. Air-Dried

The suctions of the air-dried shear test specimens were estimated based on the measured gravimetric moisture content and the corresponding characteristic curve. For LC, *w*(average) = 4.7%, corresponding to 20,000 kPa; for LS, *w*(average) = 2.4%, 2,000 kPa. Additionally, the specimens from LC exhibited some shrinkage while maintaining their integrity, yet detached from the steel mold during drying. The dimension of one specimen was measured, varying from 60 mm to 59 mm. Figure 12 shows the dispersion of points and the linear regression line adopted as corresponding to the shear strength envelope of the air-dried samples. The mean envelopes obtained from the flooded direct shear tests (8 points) resulted in c' = 43.1 kPa and ϕ' = 27.4° for LC, and c' = 75.0 kPa and ϕ' = 28.7° for LS.

Notably, the cohesion parameter shows a significant increase compared to the flooded tests. The angle of friction exhibits closer proximity between the tests. The average value of the friction angle obtained from the air-dried tests in LC is close to the end of the first quartile of friction angles determined in the statistical analysis of the flooded tests. For LS, the friction angle obtained from the air-dried tests is near the maximum values of friction angles determined in the statistical analysis of the flooded tests.

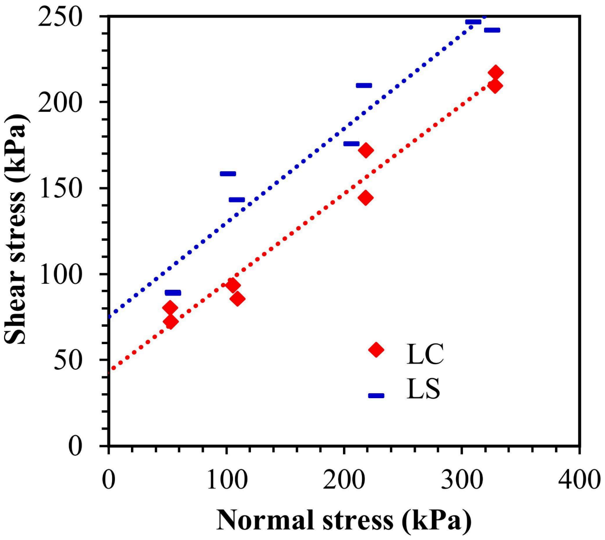

Figure 12: Shear strength envelopes for air-dried specimens.

4.4.3. Shear Strength Envelopes of Unsaturated Soils

Table 6 presents the values used for the calculations of the equations by Vilar (2006) and Vanapalli et al. (1996).

Table 6: Parameters of the unsaturated shear strength models of Vilar (2006) and Vanapalli et al. (1996).

	LC	LS
	Vilar (2006)	
tan ϕ'	0.5396	0.4791
a	1.8532	2.0875
Suction (kPa)	20000	2000
c_{ult} (air dryed) (kPa)	43.0	75.0
c'	9.8	11.5
b	0.0301	0.0147
	Vanapalli et al. (1996)	
tan ϕ'	0.5396	0.4791
θ_s (%)	59.8	38.6
θ_r (%)	5	1.5

Figure 13 shows the predicted shear strength of the unsaturated soils by the models of Vanapalli et al. (1996) and Vilar (2006) for LC and LS. The graphs display the variation of c and ϕ_b in relation to suction.

For both soils, the envelopes are only coherent at very low suction levels, around 2 kPa, close to the air-entry value of the soils. For LC, in the suction range between 5 and 77 kPa, there is an underestimation of the resistance increment of up to 16%, equivalent to 3 kPa. Here, 3 kPa is just under one-third of the effective cohesion determined for the soil. After 77 kPa of suction, the increment begins to be overestimated, reaching the same magnitude mentioned at 100 kPa.

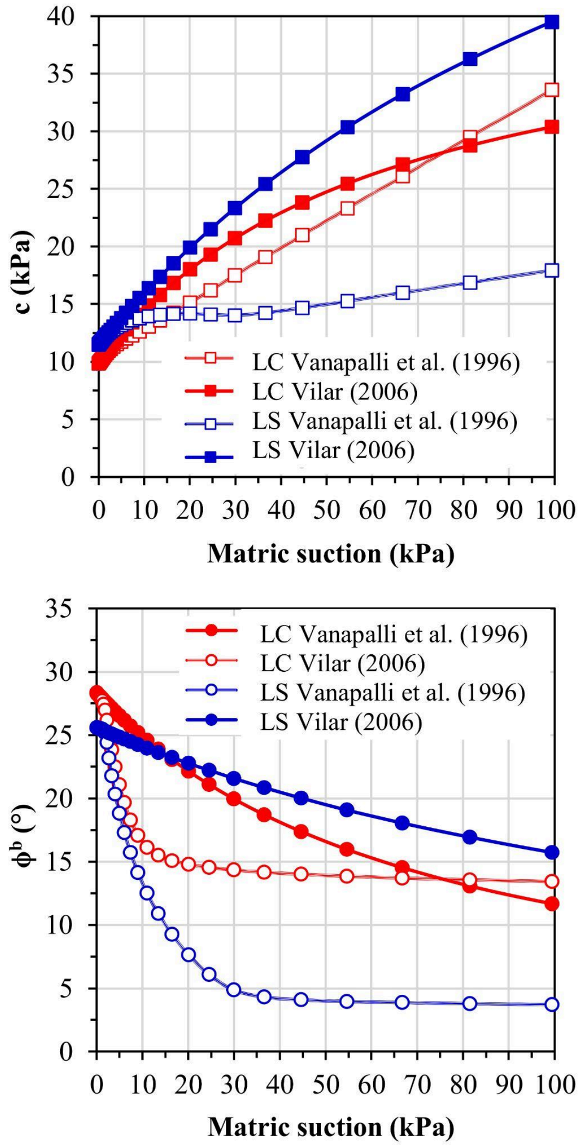

Figure 13: Predicted unsaturated shear strength using the Vanapalli et al. (1996) and Vilar (2006) models.

For LS, the inconsistency between the envelopes is even more noticeable. At 10 kPa of suction, there is a 17% underestimation of the resistance increment, 2 kPa. At 55 kPa, the underestimation is about 100%, with the value expected by the Vanapalli et al. (1996) model being half of the value expected for the Vilar

(2006) model. This discrepancy continues until 100 kPa of suction. Above 100 kPa of suction, LC starts to show values even more discordant from those observed for LS.

The ϕ^b equals ϕ' when suction approaches zero, for both models. ϕ^b also varies quite correspondingly between the models in the range of 0 to 2 kPa, the air-entry value of the two soils. Increasing the levels of suction, the Vilar (2006) model describes a smooth variation of ϕ^b reduction throughout the range up to 100 kPa of suction. For the Vanapalli et al. (1996) model, there is a marked reduction in ϕ^b between the air-entry value and approximately 10 kPa of suction for LC and 30 kPa for LS. From these points, for the Vanapalli et al. (1996) model, ϕ^b tends towards constancy and leads the linear format of resistance increment. In the Vilar model, ϕ^b tends towards zero as suction approaches infinity.

Given the considerable discrepancy between the two models studied for the two soils, efforts were made to reconcile the resistance prediction of Vanapalli et al. (1996) – feasible to apply in the software – with the resistance prediction of the Vilar (2006) model.

The equations for the increments of shear resistance of unsaturated soils due to suction for Vilar (2006), Vanapalli et al. (1996), Fredlund et al. (1978), and Bishop (1959) are as described in equations (10) to (13).

$$\frac{u_a-u_w}{a+b(u_a-u_w)} = (u_a - u_w)\left[(tg\phi')\left(\frac{\theta_w-\theta_r}{\theta_s-\theta_r}\right)\right] =$$

$$(u_a - u_w)tg\phi^b = \chi(u_a - u_w)tg\phi' \qquad (10)$$

$$\phi^b = arctg\left(\frac{1}{a+b(u_a-u_w)}\right) = arctg\left(tg\phi'\left(\frac{\theta_w-\theta_r}{\theta_s-\theta_r}\right)\right) \qquad (11)$$

$$\chi = \frac{tg\phi^b}{tg\phi'} = \left(\frac{\theta_w-\theta_r}{\theta_s-\theta_r}\right) \qquad (12)$$

Considering the relationship:

$$\chi_{Vilar}(\Psi) = \frac{tg\phi^b Vilar(\Psi)}{tg\phi'} = \left(\frac{\theta_{w\,eq}(\Psi)-\theta_r}{\theta_s-\theta_r}\right) \qquad (13)$$

Where: $\chi_{Vilar}(\Psi)$ is the parameter χ from Vilar's equation (2006) as a function of suction; $\phi^b Vilar(\Psi)$ is the ϕb from Vilar's equation (2006) as a function of suction; $\theta_{w\,eq}(\Psi)$ is the equivalent volumetric moisture content as a function of suction. The equations (14) and (15) is given:

$$\theta_{w\,eq}(\Psi) = \chi_{Vilar}(\Psi).\theta_s - \chi_{Vilar}(\Psi).\theta_r + \theta_r \qquad (14)$$

Or:

$$\theta_{w\,eq}(\Psi) = \frac{a\cdot(\theta_s-\theta_r)}{a+b(u_a-u_w)} + \theta_r \qquad (15)$$

Where $\theta_{w\,eq}(\Psi)$ can be understood as a function $\theta_w(\Psi)$, such that it enables obtaining the results of Vilar's resistance from the application of the Vanapalli et al. (1996) equation. In this context, $\theta_{w\,eq}(\Psi)$, functions as a characteristic curve for compatibility. The reconciled envelopes match accurately across the entire range of applied suction. Figure 14 shows the $\theta_{w\,eq}(\Psi)$ curves obtained for the soils of LC and LS.

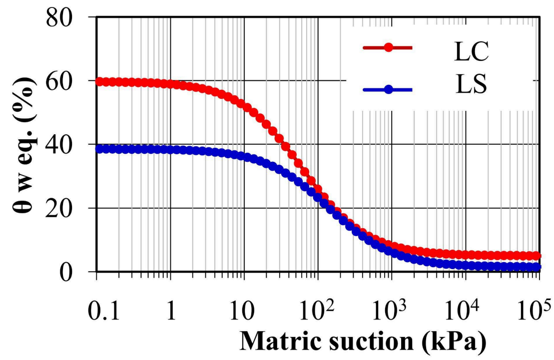

Figure 14: Compatibility characteristic curve, $\theta_{w\,eq}(\Psi)$.

4.5. Computational Analysis

The computational analyses were performed using the parameters obtained from the field investigations, laboratory tests, and numerical modeling assumptions discussed in the previous sections. Due to the large amount of data generated and employed throughout the study, Table 7 summarizes the main input parameters adopted in the numerical simulations, including hydraulic, mechanical, and boundary condition parameters used in the SEEP/W and SLOPE/W analyses.

4.5.1. Flow Analysis

Figure 15 illustrates the variation in pore pressures from a vertical subsection from the top surface of the slope. Similar patterns are observed from the base of the slope surface and perpendicular to the inclined surface of the slope body.

The general behavior of pore pressure variation is quite similar among the studied soils and consistent with other studies, despite differences in hydraulic properties (e.g., Yu et al. 2020, Liu et al. 2017). LS exhibits more pronounced wetting fronts, reaching 1.6 m in MOD1 and 2.0 m in MOD2.

The porosity, or saturated volumetric moisture content of LC, is about 50% higher compared to LS – approximately 60/40 (Table 2). Despite LC's greater total water storage capacity in its pores, the variations in water volume in the pores also show some degree of correspondence since both soils have similar air-entry values and slopes of the macropore desaturation lines.

The same initial pore pressure for both soils implies that they started from relatively similar conditions. The k_{fs} values are also very similar. This reinforces the evidence that the differences observed are related to the shape of the unsaturated conductivity curve of the soils.

It is also noteworthy that the maximum depths reached by the wetting fronts for LC were greater in MOD1 than in MOD2, and for LS, they were greater in MOD2 compared to MOD1.

Table 7: Summary of input parameters adopted in the computational analyses.

	LC		LS	
SEEP/W				
	MOD1	MOD2	MOD1	MOD2
SWCC	GF	GF	GF	GF
kfs (cm/s)	$2.3 \cdot 10^{-4}$	$2.3 \cdot 10^{-4}$	$2.7 \cdot 10^{-4}$	$2.7 \cdot 10^{-4}$
k(ψ)	PD	G	PD	G
SLOPE/W - LE				
γ (kN/m³)	16.5		20.0	
c' (kPa)	9.8		11.5	
ϕ' (°)	28.3		25.6	
USM	V		V	
SWCC	$\theta_{w\,eq}(\Psi)$		$\theta_{w\,eq}(\Psi)$	
SLOPE/W - MC				
c'				
SD (kPa)	3.45		4.54	
Min.	0.5		2.6	
Max.	17.3		21.5	
ϕ'				
SD (kPa)	1.1		1.2	
Min.	26.2		22.1	
Max.	31.1		28.6	
Correlation				
c'-ϕ'	-0.72		-0.90	

Note: GF = Gitirana & Fredlund (2004); PD = Priesack & Durner (2006); G = Gardner (1958); USM = Unsaturated Strength Model available in the software; V = Vanapalli et al. (1996); $\theta_{w\,eq}$ = Compatibility Characteristic curve used to convert the Vanapalli et al. (1996) model into the Vilar (2006) model.

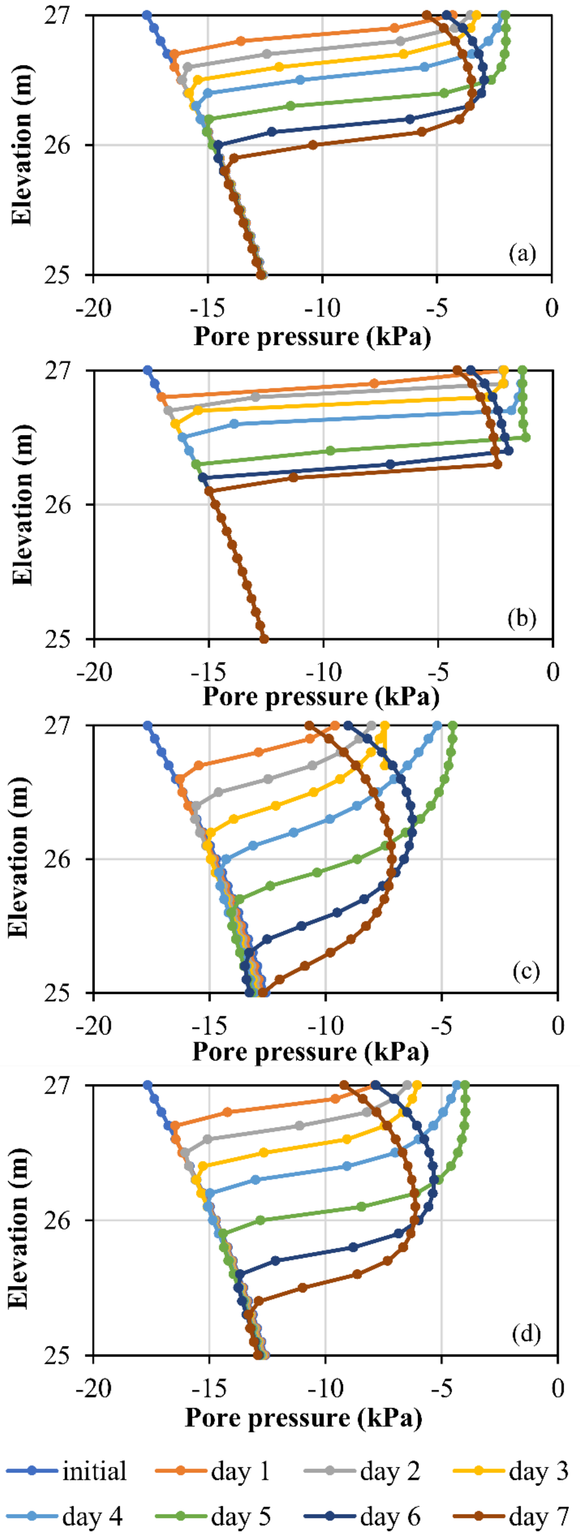

Figure 15: Variation of pore pressures due to rainwater infiltration in: (a) MOD1-LC; (b) MOD2-LC; (c) MOD1-LS; (d) MOD2-LS.

4.5.2. Stability Analysis – Factor of Safety

The Critical Surface identified by the limit equilibrium method was the same from day 0 to day 7, for all cases. It is observed that the influence of rainwater infiltration on the stability analyses of the slope models occurs through the advancement of the saturation and wetting fronts that reach the slices located at the extremities of the critical failure surfaces.

In comparison, the hydraulic models MOD1 and MOD2 exhibit very compatible behaviors with each other. The lowest Factors of Safety found were 1.1139 in MOD1 for LC and 1.0003 in MOD1 for LS. Figure 16 presents the critical failure surfaces obtained from the analyses performed using both software packages, allowing the visualization of the failure geometry and rupture depth associated with the minimum FS. The minimum FS values were observed at the end of the seventh day, coinciding with the maximum depth reached by the wetting front associated with rainwater infiltration. For context, the stability analysis of the saturated slope, under the same boundary conditions, indicates a FS of 0.933 for LC and 0.864 for LS.

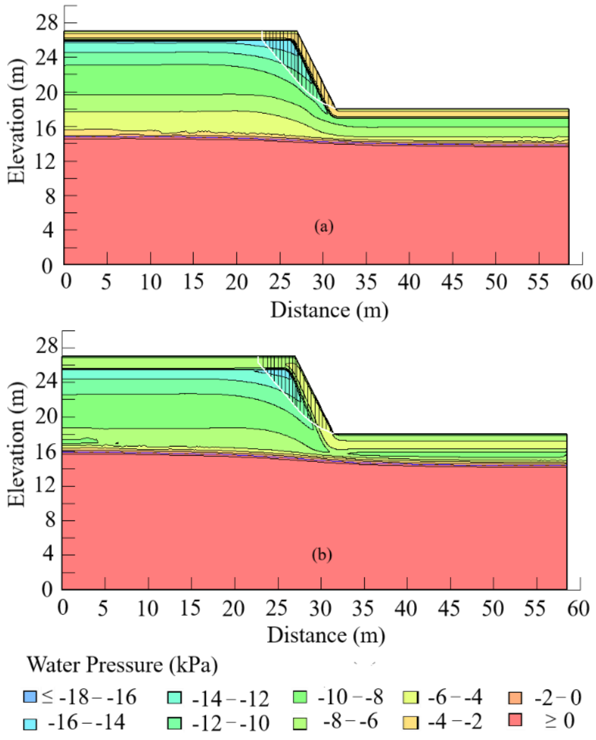

Figure 16: Critical failure surfaces. (a) MOD1-LC Day 7; and (b) MOD1-LS Day 7.

An increase in ϕ^b, from day 0 to day 7, is noted for all the affected slices due to the pore saturation process. This behavior is expected, with ϕ^b tending to ϕ' at pore pressure levels close to 0 kPa. There is also a noticeable reduction in the increase of resistance due to suction across all models, as well as a reduction in the FS, a phenomenon extensively explored in the literature, Figure 17.

4.5.3. Stability Analysis – Monte Carlo

As a complement to deterministic analyses, a probabilistic Monte Carlo analysis was conducted for the models where the lowest Factors of Safety were found: MOD1-LC and MOD1-LS, day 7. Figure 18 displays the probability density function resulting from the Monte Carlo analyses for LC and LS, respectively. Table 8 presents the parameters of the Monte Carlo analysis.

The standard deviations of the Factors of Safety for both models converged to constancy, approximately, between simulations no. 3,000 and 4,000. The average Factors of Safety found differed only in the hundredths place compared to deterministic analyses. For LC, the difference was 0.0038 and for LS, it was 0.0035.

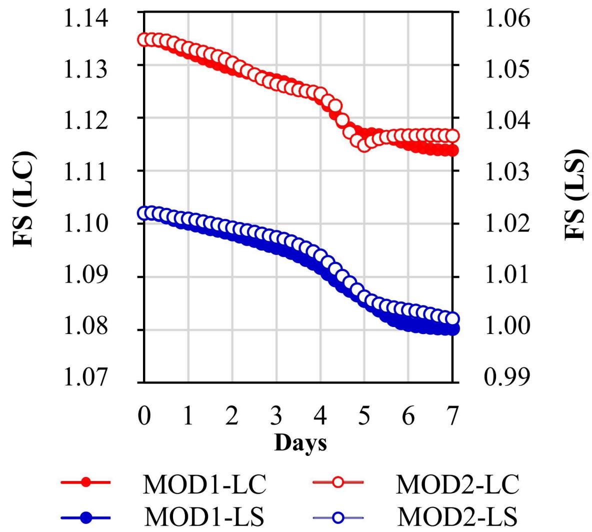

Figure 17: Variation of Factor of Safety vs. elapsed time.

Both probability density functions displayed a normal-like distribution. The range between the maximum and minimum Factors of Safety obtained was 0.392 for LC and 0.351 for LS. It is noted that the frequency of the average Factors of Safety for LC is close to 10%, while for LS, it is around 6 to 7%. It is also noted that LS has a higher standard deviation, as well as a flatter distribution appearance compared to LC. These factors are consistent expressions with the c'-ϕ' distributions determined in the study.

As with the Factors of Safety, the appropriate value of Failure Probability associated with a project depends on the consequences of failure. Failure Probability can provide a more comprehensible basis for judging what is an acceptable risk and can add significant value to the results of slope stability analyses (Duncan et al. 2014). It should be noted that the models were developed and evaluated in the context of the impacts of rainwater infiltration on stability analysis and do not necessarily represent a recommended condition for design.

The failure probability for LC was 2.28% as in 114 simulations a Factors of Safety less than 1 (FS<1) was determined. Thus, only a small portion of the left tail of the probability density function is located in the failure zone, FS<1. For LS, the failure probability was 48.38% because in 2419 simulations a Factors of Safety less than 1 was found. It is evident, then, that about half of the probability density function is within the failure zone, FS<1. Hence, the slope of LS appears much more susceptible to failure than the slope of LC.

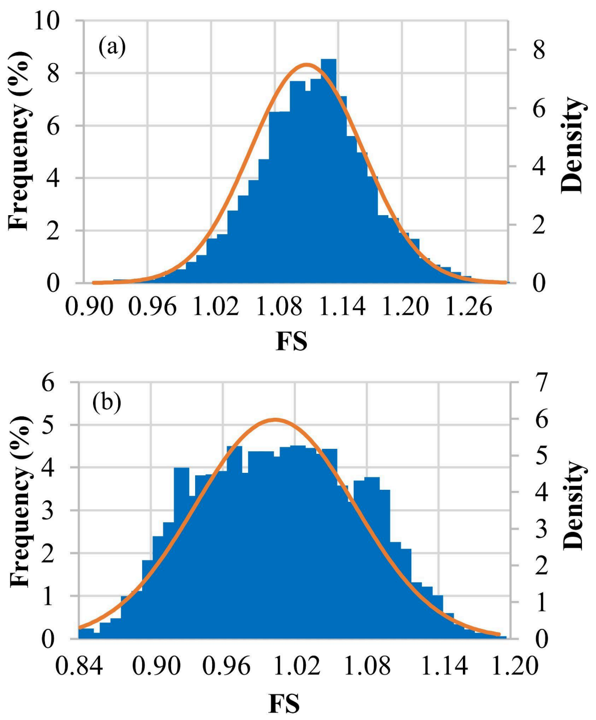

Figure 18: Normal distribution curves and histograms obtained from the Monte Carlo simulations for: (a) MOD1-LC Day 7; and (b) MOD1-LS Day 7.

Table 8: Results of probabilistic Monte Carlo analysis for MOD1-LC and MOD1-LS – Day 7.

Parameter	LC	LS
Average FS	1.110	1.004
Reliability Index	2.0659	0.0567
Probability of Failure	0.023	0.484
Standard Deviation	0.0533	0.0668
Minimum FS	0.905	0.837
Maximum FS	1.297	1.190

The reliability index is essentially related to the probability of failure and can be understood as an indicator of the number of standard deviations between failure and the most likely value of the Factors of Safety. Therefore, it can be used as an alternative measure that shows the probability of a slope remaining stable under specified conditions (Duncan et al. 2014).

Wang et al. (2011) suggest – for usual design conditions – that the failure probability ranges from 16% to 0.00003%, and the reliability index ranges from 1.0 to 5.0 respectively. Thus, a high probability of failure is associated with a low reliability index. The Reliability Index from the LC analysis was 2.0659, considered low, and from LS was 0.0567, extremely low.

The lowest Factors of Safety found in MOD1 LC (Day 7) was 0.9055, a value 0.0275 less than the 0.933 from the deterministic saturated analysis. The lowest Factors of Safety found in MOD1 LS (Day 7) was 0.8375, a value 0.0265 less than the 0.864 from the deterministic saturated analysis. It should be noted that in the deterministic saturated analysis, expected values of c' and ϕ' obtained from the statistical analysis mean of these parameters were used. The maximum Factors of Safety obtained in the probabilistic analysis were 1.2975 and 1.1904, for LC and LS, respectively. In general, the impact of the variability of resistance parameters in the stability analysis is significant, consistent with Nguyen & Likitlersuang (2019) and Huang et al. (2020).

5. Conclusions

This study advances the understanding of rainfall-induced hydromechanical behavior in Brazilian lateritic soils by providing a comparative framework between two soils of contrasting texture - one clayey, from Londrina, and one sandy, from Mandaguaçu. A central finding is that both soils exhibit hydromechanical characteristics that diverge meaningfully from those described in classical literature for generic clayey and sandy soils, reinforcing the need for region-specific characterization when assessing lateritic profiles.

The original contribution of this work is fourfold. First, it demonstrates that statistical combination of flooded direct shear test data represents a viable and resource-efficient approach to quantifying the variability of strength parameters - a practical tool for contexts with limited testing resources. Second, it proposes an equivalent characteristic curve to reconcile the incompatibility between two widely used unsaturated shear strength models, enabling more consistent use in stability software. Third, it delivers a systematic, multi-scenario evaluation of paired hydraulic and mechanical models, producing a sensitivity framework that can guide model selection in lateritic slope stability assessments. Fourth, the Monte Carlo probabilistic analysis reveals that strength parameter variability exerts a non-negligible influence on computed safety, even when deterministic factors of safety appear adequate.

This study relies on the limit equilibrium method, which does not capture coupled stress-deformation behavior or progressive failure mechanisms, and addresses infiltration from a short-term perspective that does not account for cumulative seasonal effects. The probabilistic analysis treats soil parameters as spatially uniform random variables, providing the groundwork upon which a random field approach, accounting for spatial correlation, can be built in future research.

From a practical standpoint, the results indicate that rainfall infiltration modifies pore pressures primarily within the first 1-2 m of depth, and that the sandy lateritic soil presents greater percolation capacity despite similar field-saturated permeability coefficients – a counterintuitive finding with direct implications for slope stability assessment. Taken together, these outcomes suggest that geotechnical design in tropical regions should move beyond single-value deterministic analyses and incorporate probabilistic treatment of strength parameters, particularly for soils whose behavior cannot be reliably predicted by classical frameworks.

Acknowledgement

The authors thank the Coordination of Improvement of Higher Education Personnel (CAPES) for funding the research.

Credit author statement

P.H.L.D: Conceptualization, Methodology, Investigation, Data curation, Formal analysis, Software, Visualization, Writing – original draft, Writing – review & editing.

A.D.O.: Methodology, Investigation, Writing – original draft, Writing – review & editing.

G.F.N.G.J.: Methodology, Validation, Writing – review & editing.

R.S.T.: Conceptualization, Methodology, Supervision, Project administration, Funding acquisition, Resources, Validation, Writing – review & editing.

References

ABRAMENTO M., BONATTO A.M., ABREU F.A.N., CAMPOS L.F., BELUCO R., MAION A.V., SANTOS L.M.A. 2022. Development of a landslide hazard analysis program for a 41-km railway line across "Serra do Mar" range, Brazil. Bulletin of Engineering Geology and the Environment, 82, 91. https://doi.org/10.1007/s10064-023-03106-6

ALLO E.T., SHRESTHA D.P., SUDIBYAKTO S. 2014. A slope stability assessment in the tropics. https://doi.org/10.1016/j.geomorph.2009.01.009

ALMEIDA M.A., MIGUEL M.G., TEIXEIRA S.H.C. 2011. Horizontal Bearing Capacity of Piles in a Lateritic Soil. J. Geotech. Geoenviron. Eng., 137(1): 59-69. https://doi.org/10.1061/(ASCE)GT.1943-5606.0000410

AMERICAN SOCIETY FOR TESTING AND MATERIALS - ASTM D3080-11. 2011. Standard Test Method for Direct Shear Test of Soils under Consolidated Drained Conditions. ASTM International: West Conshohocken, PA, USA, 9. https://doi.org/10.1520/D3080_D3080M-11

ASTM D5298-16. 2016. Standard test method for measurement of soil potential (suction) using filter paper. ASTM International, West Conshohocken, PA. https://doi.org/10.1520/D5298-16

ANDRADES FILHO C., MEXIAS, F.L.S. (EDITORES). 2024. WebMapa de Movimentos de Massa para equipes de apoio na situação de calamidade - RS - Maio de 2024. Lab. Latitude – CEPSRM/PPGSR/ DEGD | IGeo | UFRGS. https://arcg.is/ezjvW.

AUFLIČ M.J., BEZAK N., ŠEGINA E., FRANTAR P., GARIANO S.L., MEDVED A., PETERNEL T. 2023. Climate change increases the number of landslides at the juncture of the Alpine, Pannonian and Mediterranean regions. Research Square. https://doi.org/10.21203/rs.3.rs-3087521/v1

AUGUSTO FILHO O., FERNANDES M. 2019. A landslide analysis of unsaturated soil slopes based on rainfall and matric suction data. Bulletin of Engineering Geology and the Environment, 78(6), 4167-4185. https://doi.org/10.1007/s10064-018-1392-5

BENSON C.H., DANIEL D.E., BOUTWELL G.P. 1999. Field performance of compacted clay liners. Journal of Geotechnical and Geoenvironmental Engineering ASCE, 125(5), 390-403. https://doi.org/10.1061/(ASCE)1090-0241(1999)125:5(390)

BISHOP A.W. 1955. The use of slip circle in the stability analysis of earth slopes. Géotechnique, 5(1), 7–17. https://doi.org/10.1680/geot.1955.5.1.7

BISHOP A.W. 1959. The principle of effective stress. Teknisk Ukeblad, 106(39), 859-863.

BRANCO L.P., GOMES A.T., CARDOSO A.S., PEREIRA C.S. 2014. Natural variability of shear strength in a granite residual soil from Porto. Geotechnical and Geological Engineering, 32, 911-922. https://doi.org/10.1007/s10706-014-9768-1

CAMAPUM DE CARVALHO J., GITIRANA JR G.F.N. 2021. Unsaturated soils in the context of tropical soils. Soils and Rocks, 44(3), e2021068121. https://doi.org/10.28927/SR.2021.068121

CAVALCANTE E.H., DANZIGER F., GIACHETI H, COUTINHO R., SOUZA A. 2007. Campos Experimentais Brasileiros. Geotecnia, 111, p. 99-205. https://doi.org/10.14195/2184-8394_111_3

CHANDLER R., CRILLY M., MONTGOMERY-SMITH M. 1992. A low-cost method of assessing clay desiccation for low-rise buildings. Proceedings of the Institution of Civil Engineers, 92(2), 82–89. https://doi.org/10.1680/icien.1992.18771

CHERUBINI C. 2000 Reliability evaluation of shallow foundation bearing capacity on c′, φ′ soils. Canadian Geotechnical Journal, 37, 264–269. https://doi.org/10.1139/t99-096

CHRISTONI A.R.F., TEIXEIRA R.S., BRANCO C.J.M.C. 2019. Failure load of small diameter piles excavated with manual auger in a tropical collapsible soil. Geotecnia 146, pp. 71-93. http://doi.org/10.24849/j.geot.2019.146.04

COMEGMA L., PICARELLI L., BUCCHIGNANI E., MERCOGLIANO P. 2013. Potential effects of incoming climate changes on the behaviour of slow active landslides in clay. Landslides, 10, 373–391. https://doi.org/10.1007/s10346-012-0339-3

DI MATTEO L., VALIGI D., RICCO R. 2013. Laboratory shear strength parameters of cohesive soils: variability and potential effects on slope stability. Bulletin of Engineering Geology and the Environment, 72(1), 101–106. https://doi.org/10.1007/s10064-013-0459-6

DI MATTEO L., VALIGI D., RICCO R., ROMEO S. 2015. Effect of laboratory repeatability of direct shear test on slope stability. In: Schweckendiek T, et al. (Eds.) Geotechnical Safety and Risk V, pp. 808-812. IOS Press Ebooks. https://doi.org/10.3233/978-1-61499-580-7-808

DUNCAN J.M., WRIGHT S.G., BRANDON T.L. 2014. Soil strength and slope stability, 2nd ed. John Wiley & Sons, New Jersey.

DUNCAN M. 2000. Factors of safety and reliability in geotechnical engineering. Journal of Geotechnical and Geoenvironmental Engineering ASCE, 126(4), 307-316. https://doi.org/10.1061/(ASCE)1090-0241(2000)126:4(307)

DURNER W. 1994. Hydraulic conductivity estimation for soils with heterogeneous pore structure. Water Resources Research, 30(2), 211–223. https://doi.org/10.1029/93WR02676

EBRAHIMI-B N., GITIRANA JR, G., FREDLUND D., FREDLUND M., SAMARASEKERA L. 2004. A lower limit for the water permeability coefficient. In: 57th Canadian Geotechnical Conference and the 5th Joint CGS-IAH Conference Session E (pp. 12-19), Quebec, Canadá.

FEKI M., RAVAZZANI G., BARONTINI S., CEPPI A., MANCINI M. 2020. A comparative assessment of the estimates of the saturated hydraulic conductivity of two anthropogenic soils and their impact on hydrological model simulations. Soil and Water Research, 15(3), 135-147. https://doi.org/10.17221/33/2019-SWR

FENTON G.A., GRIFFITHS D.V. 2008. Risk assessment in geotechnical engineering. Wiley, Hoboken. https://doi.org/10.1002/9780470284704

FERNANDES M.A. 2016. Study of the mechanisms of instability in an unsaturated sandy soil slope located in the Midwest Paulista region. (Doctoral dissertation). Escola de Engenharia de São Carlos, Universidade de São Paulo, São Carlos, Brazil.

FINK H. 2018. Permeability of sandy soils in natural and compacted states in variable load permeameters with flexible walls. (Undergraduate thesis). Universidade Estadual de Londrina, Londrina, Brazil. [in Portuguese]

FREDLUND D.G., MORGENSTERN N.R., WIDGER R.A. 1978. The shear strength of unsaturated soils. Canadian Geotechnical Journal, 15(3), 313–321. https://doi.org/10.1139/t78-029

FREDLUND D.G., RAHARDJO H., FREDLUND M.D. 2012. Unsaturated soil mechanics in engineering practice. John Wiley & Sons, New Jersey.

GARDNER W.R. 1958. Some steady state solutions of the unsaturated moisture flow equation with application to evaporation from a water table. Soil Science, 85(4), 228-232. https://doi.org/10.1097/00010694-195804000-00006

GEOSTUDIO. 2020a. SEEP/W Heat and mass transfer modeling with Geostudio. GeoSlope International Ltd.: Calgary, Alberta, Canada.

GEOSTUDIO. 2020b. SLOPE/W Stability Modeling with GeoStudio. Geo-Slope International Ltd.: Calgary, Alberta, Canada.

GHEZZEHEI T.A., KNEAFSEY T.J., SU G.W. 2007. Correspondence of the Gardner and van Genuchten–Mualem relative permeability function parameters. Water Resources Research, 43(10), W10417. https://doi.org/10.1029/2006WR005339

GIDIGASU M.D. 1976. Laterite soil engineering: pedogenesis and engineering principles. Elsevier Scientific Publishing Company, Amsterdam, 554pp.

GITIRANA JR G.F.N., FREDLUND D.G. 2004. Soil-water characteristic curve equation with independent properties. Journal of Geotechnical and Geoenvironmental Engineering, 130(2), 209–212. https://doi.org/10.1061/(ASCE)1090-0241(2004)130:2(209)

GITIRANA JR G.F.N., FREDLUND D.G. 2016. Statistical assessment of hydraulic properties of unsaturated soils. Soils and Rocks, 39(1), 81-95. https://doi.org/10.28927/SR.391081

GOMES A.S., LICHT O.A.B., VASCONCELLOS E.M.G., SOARES J.S. 2018. Chemostratigraphy and evolution of the Paraná Igneous Province volcanism in the central portion of the state of Paraná, Southern Brazil. Journal of Volcanology and Geothermal Research, 355, 253–269. https://doi.org/10.1016/j.jvolgeores.2017.09.006

GRECO V.R. 2016. Variability and correlation of strength parameters inferred from direct shear tests. Geotechnical and Geological Engineering, 34, 585–603. https://doi.org/10.1007/s10706-015-9968-3

GUILLAUME B., BOUKDIBA H.A., BAKKER G., BIEGANOWSKI A., BROSTAUX Y., CORNELIS W., DURNER W., HARTMANN C., IVERSEN B.V., JAVAUX M., INGWERSEN J., LAMORSKI K., LAMPARTER A., MAKÓ A., SORIANO A.M.M., MESSING I., NEMES A., POMES-BORDEDEBAT A., VAN DER PLOEG M., WEBER T.K.D., WEIHERMÜLLER L., WELLENS J., DEGRÉ A. 2023. Reproducibility of the wet part of the soil water retention curve: a European interlaboratory comparison. Soil. https://doi.org/10.5194/soil-9-365-2023

HUANG M.L., SUN D.A., WANG C.H., KELETA Y. 2020. Reliability analysis of unsaturated soil slope stability using spatial random field-based Bayesian method. Landslides, 18(1), 1-13. https://doi.org/10.1007/s10346-020-01525-0

HUANG R., LI W. 2011. Formation, distribution and risk control of landslides in China. Journal of Rock Mechanics and Geotechnical Engineering, 3(2), 97–116. https://doi.org/10.3724/SP.J.1235.2011.00097

HUAXIANG Y., ZHANG J., MONDAL S.K., WANG B-D., ZHOU L., WANG L., LIN Q. 2023. Projected rainfall-triggered landslide susceptibility changes in the Hengduan Mountain Region, Southwest China under 1.5–4.0 °C warming scenarios based on CMIP6 models. Atmosphere. https://doi.org/10.3390/atmos14020214

HUFF F.A. 1967. Time distribution of rainfall in heavy storms. Water Resources Research, 3(4), 1007-1019. https://doi.org/10.1029/WR003i004p01007

HUVAJ N., OĞUZ E.A. 2018. Probabilistic slope stability analysis: A case study. Sakarya University Journal of Science, 22(5), 1458–1465. https://doi.org/10.16984/saufenbilder.430032

IAT – INSTITUTO ÁGUA E TERRA. 2021. Sistema de Informações Hidrológicas (SIH). Curitiba: IAT, [2020-2021]. https://www.iat.pr.gov.br/Pagina/Sistema-de-Informacoes-Hidrologicas

KLOSE M., MAURISCHAT P., DAMM B. 2016. Landslide impacts in Germany: A historical and socioeconomic perspective. Landslides 13(1): 183-199. https://doi.org/10.1007/s10346-015-0643-9

KOCH J., SVENNEVIG K., TRIMBUR D., YARAHMADI J. 2023. Assessing the impact of climate change to landslides using public data, a case study from Vejle, Denmark. Natural Hazards and Earth System Sciences Discussions. https://doi.org/10.5194/nhess-2023-68

KOCH G.S., LINK R.F. 2002. Statistical analysis of geological data. Courier Dover Publications, USA.

LI D-Q., WANG L., CAO Z-J., QI X-U. 2019. Reliability analysis of unsaturated slope stability considering SWCC model selection and parameter uncertainties. Engineering Geology, 260, 105207. https://doi.org/10.1016/j.enggeo.2019.105207

LICHT O.A.B.; ARIOLI E.E. 2018. Mapa geológico do Grupo Serra Geral no estado do Paraná. Instituto Água e Terra, Curitiba. http://www.iat.pr.gov.br/Pagina/Mapeamento-Geologico#

LICHT O.A.B., ARIOLI E.E. 2020. A photographic atlas of the architecture, flow geometry and morphology, and facies of Serra Geral Group (Paraná Igneous Province) in the State of Paraná, Brazil. Boletim Paranaense de Geociências, 76(1), 1–69. https://doi.org/10.5380/geo.v76i0.78536

LIN H., ZHONG W. 2019. Influence of rainfall intensity and its pattern on the stability of unsaturated soil slope. Geotechnical and Geological Engineering, 37(2), 615–623. https://doi.org/10.1007/s10706-018-0631-7

LIN W., FUKUHARA M., UCHIMURA T., GALLAGE C., ABEYKOON T. 2020. An EWS of landslide and slope failure by MEMS tilting sensor array. In: Proceedings of the 2nd International Symposium on Computational Geomechanics. https://doi.org/10.1007/978-3-030-60311-3_35

LIU W., LUO X., HUANG F., FU M. 2017. Uncertainty of the soil–water characteristic curve and its effects on slope seepage and stability analysis under conditions of rainfall using the Markov Chain Monte Carlo method. Water, 9(758), w9100758. https://doi.org/10.3390/w9100758

LIU X., WANG Y., LEUNG A.K. 2023. Probabilistic back analysis of rainfall-induced slope failure considering slope survival records from past rainfall events. Computers and Geotechnics, 159, 105436. https://doi.org/10.1016/j.compgeo.2023.105436

LU M., ZHANG J., ZHENG J., YU Y. 2022. Assessing annual probability of rainfall-induced slope failure through a mechanics-based model. Acta Geotechnica, 17, 949–964. https://doi.org/10.1007/s11440-021-01278-7

LU N. 2016. Generalized soil water retention equation for adsorption and capillarity. Journal of Geotechnical and Geoenvironmental Engineering, 142(10), 04016051. https://doi.org/10.1061/(ASCE)GT.1943-5606.0001524

MALAYA C., SREEDEEP S. 2012. Critical review on the parameters influencing soil-water characteristic curve. Journal of Irrigation and Drainage Engineering, 138(1), 55–62. https://doi.org/10.1061/(ASCE)IR.1943-4774.0000371

MARINHO F.A.M., OLIVEIRA O.M. 2006. The filter paper method revised. ASTM Geotechnical Testing Journal, 29(3), 250-258. https://doi.org/10.1520/GTJ14125

MAYUMI C.M., HIRYE D., SALAS A.A, FILARDO A.S., MCPHEARSON T., WAGNER F. 2023. Assessing landslide drivers in social-ecological-technological systems: the case of metropolitan region of São Paulo, Brazil. Remote Sensing. https://doi.org/10.3390/rs15123048

KARIM M.R., HUGHES D., RAHMAN M.M. 2022. Unsaturated hydraulic conductivity estimation—A case study modelling the soil-atmospheric boundary interaction. Processes, 10(7), 1306. https://doi.org/10.3390/pr10071306

MIGUEL M.G., VILAR O.M. 2009. Study of the water retention properties of a tropical soil. Canadian Geotechnical Journal, 46(9), 1084-1092.
https://doi.org/10.1139/T09-039
NG C.W.W., WANG B., TUNG Y. 2001. Three-dimensional numerical investigations of groundwater responses in an unsaturated slope subjected to various rainfall patterns. Canadian Geotechnical Journal, 38, 1049–1062.
https://doi.org/10.1139/t01-057
NGUYEN T.S., LIKITLERSUANG S. 2019. Reliability analysis of unsaturated soil slope stability under infiltration considering hydraulic and shear strength parameters. Bulletin of Engineering Geology and the Environment, 78(8), 5727–5743.
https://doi.org/10.1007/s10064-019-01513-2
NIELSEN D.R., BIGGAR J.W., ERH K.T. 1973. Spatial variability of field-measured soil-water properties. Hilgardia, 42(7), 215-260.
https://doi.org/10.3733/hilg.v42n07p215
NITSCHE P.R., CARAMORI P.H., RICCE W.S., PINTO L.F.D. 2019. Atlas Climático do Estado do Paraná. Instituto Agronômico do Paraná - IAPAR, Londrina. Available in: https://www.idrparana.pr.gov.br/system/files/publico/agrometeorologia/atlas-climatico/atlas-climatico-do-parana-2019.pdf
NOGAMI J.S., VILLIBOR D.F. 1980. Caracterização e classificação gerais de solos para pavimentação: limitações do método tradicional, apresentação de uma nova sistemática. In: Reunião Anual de Pavimentação, 15., Belo Horizonte.
OLIVEIRA A.D. 2023. Numerical and analytical evaluation of rainwater infiltration in lateritic clay soil profile. Doctoral Thesis. Programa de Pós-Graduação em Engenharia Civil, Universidade Estadual de Londrina, 204 l.
OLIVEIRA A.D., PELAQUIM F.G.P., ZANIN R.F.B., MELO T.R., TAVARES FILHO J., ANDRELLO A.C., TEIXEIRA R.S. 2022. The structure of tropical lateritic soils as an impacting factor in the shape of soil-water characteristic curves. Soils and Rocks, 45(2), e2022070521. https://doi.org/10.28927/SR.2022.070521
OSAKO L.S. 2021. Updating landslide inventory maps using high resolution digital orthophotos and digital surface and elevation modeling: the case study of Brusque city, Santa Catarina state, Brazil. ISPRS Annals of the Photogrammetry, Remote Sensing and Spatial Information Sciences.
https://doi.org/10.5194/ISPRS-ANNALS-V-3-2021-251-2021
OSINUBI K.J., NWAIWU C.M. 2006. Design of compacted lateritic soil liners and covers. Journal of Geotechnical and Geoenvironmental Engineering, 132(2), 203–213.
https://doi.org/10.1061/(ASCE)1090-0241(2006)132:2(203)
PANDE P.B., KHANDESHWAR S.R., BAJAD S.P. 2021. Shear strength behavior of an unsaturated clayey soil. Lecture Notes in Civil Engineering. 483–492.
https://doi.org/10.1007/978-981-33-6370-0_43
PATIL U.D., PUPPALA A.J., HOYOS L.R., PEDARLA A. 2017. Modeling critical-state shear strength behavior of compacted silty sand via suction-controlled triaxial testing. Engineering Geology, 231, 21–33.
https://doi.org/10.1016/j.enggeo.2017.10.011
PEI Y., QIU H., YANG D., LIU Z., MA S., LI J., CAO M., WUFUER W. 2023. Increasing landslide activity in the Taxkorgan River Basin (eastern Pamirs Plateau, China) driven by climate change. Catena.
https://doi.org/10.1016/j.catena.2023.106911
PHAM T.A., MELIS S. 2022. Disturbed state concept and non-isothermal shear strength model for unsaturated soils. Bulletin of Engineering Geology and the Environment, 81(5).
https://doi.org/10.1007/s10064-022-02688-x
PRIESACK E., DURNER W. 2006. Closed-form expression for the multi-modal unsaturated conductivity function. Vadose Zone Journal, 5(1), 121-124.
https://doi.org/10.2136/vzj2005.0066
RAHARDJO H., KIM Y., SATYANAGA A. 2019. Role of unsaturated soil mechanics in geotechnical engineering. International Journal of Geo-Engineering, 10(8), 1–23.
https://doi.org/10.1186/s40703-019-0104-8
RAHARDJO H., ONG T.H., REZAUR R.B., LEONG E.C. 2007. Factors controlling instability of homogeneous soil slopes under rainfall. Journal of Geotechnical and Geoenvironmental Engineering, 133(12), 1532-1543.
https://doi.org/10.1061/(ASCE)1090-0241(2007)133:12(1532)
REYNOLDS W.D. 2008. Chapter 76 saturated hydraulic properties: well permeameter. In: Carter MR, Gregorich EG (Eds.), Soil Sampling and Methods of Analysis (2nd ed., pp. 1025-1042). Taylor & Francis Group, Boca Raton, FL.
REYNOLDS W.D., ELRICK D.E. 1986. A method for simultaneous in situ measurement in the vadose zone of field saturated hydraulic conductivity, sorptivity and the conductivity-pressure head relationships. Ground Water Monitoring Remediation, 6(1), 84-95.
https://doi.org/10.1111/j.1745-6592.1986.tb01229.x
RIENZNER M., GANDOLFI C. 2014. Investigation of spatial and temporal variability of saturated soil hydraulic conductivity at the field-scale. Soil & Tillage Research, 135, 28–40.
https://doi.org/10.1016/j.still.2013.08.012
RODRIGUEZ T.T., WEISS L.A., TEIXEIRA R.S., BRANCO C.J.M.C. 2015. Permeabilidade de solo laterítico por diferentes métodos. Semina: Ciências Exatas e Tecnológicas, 36(2), 17-32.
https://doi.org/10.5433/1679-0375.2015v36n2p17
SÁ I.S., FORTES E., PRESTES B.M.M., ROQUE D.C., GRZEGORCZYK V. 2021. Aspectos texturais e estruturas sedimentares de litofácies de uma seção geológica complementar da formação Goio Êre (Grupo Caiuá). Brazilian Journal of Development, 7(5), 46658-46675.
https://doi.org/10.34117/bjdv7n5-193
SALVATI P., BIANCHI C., ROSSI M., GUZZETTI, F. 2010. Societal landslide and flood risk in Italy, Nat. Hazards Earth Syst. Sci., 10, 465–483.
https://doi.org/10.5194/nhess-10-465-2010
SIACARA A.T., NAPA-GARCÍA G.F., BECK A.T., FUTAI M.M. 2020. Reliability analysis of earth dams using direct coupling. Journal of Rock Mechanics and Geotechnical Engineering, 12, 366-380.
https://doi.org/10.1016/j.jrmge.2019.07.012
SIACARA A.T., NAPA-GARCÍA G.F., BECK A.T., FUTAI M.M. 2024. Reliability Analysis of an Earth Dam Under Rainfall Effects. International Journal of Geosynthetics and Ground Engineering, 10(59), 1-17.
https://doi.org/10.1007/s40891-024-00571-1
SOULIE M., MONTES P., SILVEST V. 1990. Modelling spatial variability of soil parameters. Canadian Geotechnical Journal, 27, 617-630.
https://doi.org/10.1139/t90-076
SOUSA R.V.B., CELLIGOI A. 2011. Avaliação da condutividade hidráulica do solo em área agrícola e florestada na cidade de Londrina (PR) através do permeâmetro Guelph. Boletim de Geografia, 29(2), 123-133.
https://doi.org/10.4025/bolgeogr.v29i2.11184
SOUZA W.A.R., PEREIRA S.A.S., MENDES T.A., COSTA R.F., GITIRANA JR G.F.N., REBOLLEDO J.F.R. 2022. Statistical evaluation of testing conditions on the saturated hydraulic conductivity of Brazilian lateritic soils using artificial intelligence approaches. Scientific Reports, 12, 20381.
https://doi.org/10.1038/s41598-022-24779-1
SUN D., YOU G., ANNAN Z., DAICHAO S. 2016. Soil–water retention curves and microstructures of undisturbed and compacted Guilin lateritic clay. Bulletin of Engineering Geology and the Environment, 75, 781–791.
https://doi.org/10.1007/s10064-015-0765-2
TEIXEIRA R.S., PINESE J.P.P. 2006. Potencial de utilização do estrato superior do solo laterítico da cidade de Londrina, estado do Paraná, como material de apoio de aterros sanitários. Acta Scientiarum. Technology, 28(1), 85-92.
https://doi.org/10.4025/actascitechnol.v28i1.1291
VAN GENUCHTEN M.T. 1980. A closed-form equation for predicting the hydraulic conductivity of unsaturated soils. Soil Science Society of America Journal, 44(5), 892–898.
https://doi.org/10.2136/sssaj1980.03615995004400050002x
VANAPALLI S.K., FREDLUND D.G., PUFAHL D.E., CLIFTON A.W. 1996. Model for the prediction of shear strength with respect to soil suction. Canadian Geotechnical Journal, 33(3), 379-392.
https://doi.org/10.1139/t96-060
VILAR O.M. 2006. A simplified procedure to estimate the shear strength envelope of unsaturated soils. Canadian Geotechnical Journal, 43(10), 1088–1095.

https://doi.org/10.1139/t06-055
WANG L., WU C., GU X., LIU H., MEI G., ZHANG W. 2020. Probabilistic stability analysis of earth dam slope under transient seepage using multivariate adaptive regression splines. Bulletin of Engineering Geology and the Environment, 79, 2763–2775.
https://doi.org/10.1007/s10064-020-01730-0
WANG Y., AKEJU O.V. 2016. Quantifying the cross-correlation between effective cohesion and friction angle of soil from limited site-specific data. Soils and Foundations, 56, 1055-1070.
https://doi.org/10.1016/j.sandf.2016.11.009
WANG Y., CAO Z., AU S-K. 2011. Practical reliability analysis of slope stability by advanced Monte Carlo simulations in a spreadsheet. Canadian Geotechnical Journal, 48, 162–172.
https://doi.org/10.1139/T10-044
WALKINSHAW J. 1992. Landslide correction costs on US state highway systems, Transp. Res. Rec. 1343: 36–41.
WU X.Z. 2015. Modelling dependence structures of soil shear strength data with bivariate copulas and applications to geotechnical reliability analysis. Soils and Foundations, 55(5), 1243–1258.
https://doi.org/10.1016/j.sandf.2015.09.023
XAVIER J.P.S., LUIZ F.R., NERY T.D. 2022. Landslides in the state of Pernambuco. Mercator. 21, https://doi.org/10.4215/rm2022.e21003
YEH H.F., WANG J., SHEN K., LEE C. 2015. Rainfall characteristics for anisotropic conductivity of unsaturated soil slopes. Environmental Earth Sciences, 73(12), 8669–8681.
https://doi.org/10.1007/s12665-015-4032-4
YU S., REN X., ZHANG J., WANG H., ZHANG Z. 2020. Sensibility analysis of the hydraulic conductivity anisotropy on seepage and stability of sandy and clayey slope. Water, 12(1), 277.
https://doi.org/10.3390/w12010277
ZANIN R.F.B., PADILHA A.C.C., PELAQUIM F.G.P., GUTIERREZ N.H.M., TEIXEIRA R.S. 2021. The effect of pH and electrical conductivity of the soaking fluid on the collapse of a silty clay. Soils and Rocks, 44(4):e2021061620. https://doi.org/10.28927/SR.2021.061620
ZENG L., BIAN H., SHI Z., HE Z. 2017. Forming condition of transient saturated zone and its distribution in residual slope under rainfall conditions. Journal of Central South University, 24(8), 1866-1880.
https://doi.org/10.1007/s11771-017-3594-6
ZHANG L.L., FREDLUND D.G., FREDLUND M., WILSON G.W. 2014. Modeling the unsaturated soil zone in slope stability analysis. Canadian Geotechnical Journal, 51(12), 1384–1398.
https://doi.org/10.1139/cgj-2013-0394
ZHANG Z.F., GROENEVELT P.H., PARKIN G.W. 1998. The well-shape factor for the measurement of soil hydraulic properties using the Guelph Permeameter. Soil & Tillage Research, 49, 219-221.
https://doi.org/10.1016/S0167-1987(98)00174-3
ZHOU X., WEN H., ZHANG Y., XU J., ZHANG W. 2021. Landslide susceptibility mapping using hybrid random forest with GeoDetector and RFE for factor optimization. Geoscience Frontiers, 12, 101211, 1-19.
https://doi.org/10.1016/j.gsf.2021.101211
ZHOU Y., LI M., CHEN Z., HE F. 2022. Stability analysis of unsaturated soil slope under rainfall infiltration. CRC Press eBooks 307–314.
https://doi.org/10.1201/9781003330172-43

[1]Recebido 31 de outubro de 2025
Aceito 29 de junho de 2026